ENERGY DISTRIBUTIONS OF SPUTTERED NEUTRALS

AND

ELECTRON TRANSFER AND REACTIVE IONIZATION

IN ATOM-MOLECULE COLLISIONS

ENERGY DISTRIBUTIONS OF SPUTTERED NEUTRALS

AND

ELECTRON TRANSFER AND REACTIVE IONIZATION

IN ATOM-MOLECULE COLLISIONS

academisch proefschrift

ter verkrijging van de graad van Doctor in de Wiskunde en Natuurwetenschappen aan de Universiteit van Amsterdam, op gezag van de Rector Magnificus, Dr. A. de Froe, hoogleraar in de Faculteit der Geneeskunde, in het openbaar te verdedigen in de Aula der Universiteit (tijdelijk Lutherse kerk, ingang Singel 411, hoek Spui) op woensdag 18 september 1974, des namiddags te vier uur

door

GÜNTHER PETER KÖNNEN

geboren te Amsterdam

Promotor : Prof. dr. J. Kistemaker

Co-promotor: Dr. A.E. de Vries

Co-referent: Prof. dr. G. de Vries

Aan mijn ouders

Aan Ineke

V O O R W O O R D

Bij het gereedkomen van dit proefschrift wil ik allen bedanken die aan de totstandkoming ervan hebben meegewerkt.

Dit geldt in de eerste plaats mijn promotor, prof. dr. J. Kistemaker, de directeur van dit Insituut. Zijn voortdurende belangstelling voor het onderzoek is een grote stimulans voor mij geweest. Prof. dr. G. de Vries dank ik voor zijn bereidwilligheid als co-referent op te treden.

Dr. A.E. de Vries, leider van de groep Molecuulfysica, heeft gedurende al deze jaren de supervisie gehad over het onderzoek. De vele discussies die ik met hem mocht voeren, hebben in hoge mate bijgedragen tot mijn wetenschappelijke vorming. Grote bewondering heb ik ook altijd gehad voor de wijze waarop hij leiding geeft aan de groep. Het is zeker niet in de laatste plaats zijn werk, dat in de groep Molecuulfysica die bijzonder goede onderlinge verstandhouding heerst die zo onontbeerlijk is voor dit soort onderzoek.

De interesse, die prof. dr. J. Los altijd getoond heeft voor het onderzoek, is voor mij een grote steun geweest.

Dr. H.E. Roosendaal dank ik voor de vele discussies, die ik met hem heb gevoerd en die mij de weg hebben gewezen in het sputtervak.

Aan de wijze waarop ik heb kunnen samenwerken met de mensen die direct bij het experiment betrokken waren, te weten A. Haring en drs. F. Eerkens, zal ik ongetwijfeld lang goede herinneringen bewaren. Een hoogtepunt in deze periode vormde voor ons allen zeker de korte, doch stormachtige tijd dat dr. J. Grosser bij het apparaat gevoegd was. Hierbij komt de samenwerking met dr. A. Tip, die behalve aangenaam ook zeer leerzaam is geweest.

Zonder de medewerking van de uitstekende technische groepen in dit Instituut zou een onderzoek als dit niet mogelijk zijn. Van de Instrumentmakerij, onder leiding van A.F. Neuteboom, wil ik zonder de anderen hierbij te kort te doen, W.J. Barsingerhorn, R. Boddenberg, P.Th. Keâ, W.F. Peters, H. van der Veen, C.van der Zweep en ook G.A. de Ruyter bijzonder danken voor het vele werk dat zij verricht hebben.

Van het electronisch lab, onder leiding van P.J. van Deenen

gaat mijn bijzondere dank uit naar C.J. Bruyn, die zorg heeft gedragen voor de automatisering van het apparaat, alsmede naar H.A. Dekker en J. ter Horst.

Wat betreft de tekenkamer, onder leiding van E. de Haas, gaat mijn speciale dank uit naar A.P. de Jongh en M. Hoogervorst.

Tevens wil ik iedereen bedanken die een aandeel heeft gehad in de afwerking van het proefschrift. Mevr. C.J. Köke-van der Veer en mevr. M. Veldhuizen dank ik voor het uitstekende typewerk, F.L. Monterie en Th. van Dijk voor het fotografische werk en mevr. M.M. Turksma-Cabanas voor het tekenwerk. H.A. Okhuizen dank ik voor het offset drukken van het proefschrift.

Tot slot bedank ik allen binnen en buiten het FOM-Instituut die niet met name genoemd zijn maar met hun hulp een bijdrage hebben geleverd.

The work described in this thesis is part of the research program of the "Stichting voor Fundamenteel Onderzoek der Materie" (Foundation for Fundamental Research on Matter - F.O.M.) and was made possible by financial support from the "Nederlandse Organisatie voor Zuiver-Wetenschappelijk Onderzoek" (Netherlands Organization for pure Scientific Research - ZWO)

CONTENTS

INTRODUCTION

Two subjects are discussed in this thesis. The first one concerns the ejection of neutral particles from solids by sputtering, the second one concerns ionizing atom-molecule collisions in the electronvolt energy range. Although these fields have very little physical relationship, there are distinct technical connections between them. Sputtering of solids results in the emission of atoms with hyperthermal energies. Since in principle all materials can be sputtered, this is a universal way to make atomic beams in this energy range. On the other hand, sputtered beams may contain also a component of excited atoms and polyatomic particles. Since for collisional experiments the colliding systems have to be well defined, knowledge is required about the composition of sputtered beams. Information about this can be obtained by collisional ionization experiments of sputtered particles with various thermal gases. This represents a second connection between these fields.

The primary purpose of this work was to extend the sputtering technique to various elements for chemical research and to apply it explicitly to collisional ionization experiments. Most of the work in this field has been done with beams of the easily detectable alkali atoms, colliding with particles with a high electron affinity. In such systems, an electron jump requires little energy, and therefore the ionization takes place at a large internuclear separation. This ionization process, having a large cross section, can be considered to be the first step of a chemical reaction. A basic question is now, in how far these processes are important in systems in which the electron jump is not so easy. Furthermore, if colliding particles approach closely there might be a relatively large cross section for reactive ionization. For chemical research it is important to know the relevance of these processes with respect to simple charge exchange.

An important category of projectiles for chemical research are the halogen atoms. Therefore we first focussed our attention to this chemical group, and investigated the possibility for generating hyperthermal atomic halogen beams by sputtering.

In principle, hyperthermal halogen beams can be obtained by sputtering from halogen solids. In practice however, this method

is quite complicated since for this the target has to be kept at liquid nitrogen temperature. Therefore we investigated the possibility to obtain these beams by sputtering from compounds. Sputtered beams from alkalihalides were analyzed by mass spectroscopy as a function of the velocity, as described in chapter I. From these measurements we concluded that this method is indeed suited for the production of well defined halogen beams with energies above a few eV. Below this energy, the sputtered beams contain an important fraction of molecular aggregates. To get a better insight in the sputter process, we developed a model for clusterformation by sputtering, and compared it with the experimental results. This investigation, described in chapter II, became the second line in the research program.

Contrary to the alkali atoms, non-alkali beams are in general difficult to detect. For the halogen atoms however, having a large electron affinity, negative surface ionization seemed to be a promising detection possibility. We tried to detect hyperthermal halogen atoms in this way, and found a drastic increase of the ionization efficiencies at eV energies, as is described in chapter III.

The actual application of the sputtered halogen beams for collisional ionization research is described in chapter IV. Beams of organic molecules are crossed with the sputtered halogens in the ion source of a mass spectrometer to investigate the importance of ionization processes in these systems. The main research has been done with aniline molecules, since this molecule has a relatively low ionization potential and we therefore expected the largest cross section. In all cases however it was found that ion pair formation takes place, although with a considerably lower cross section than in alkali-halogen collisions. Part of the positive organic molecular ions break up into fragments; the resulting smaller ions were the same as in electron bombardment and photoionization. No trace however was found of reactive ionization.

This latter result led us to the conclusion that reactive ionization might be more likely in systems with strong covalent forces. We therefore extended the sputtering technique to carbon and studied ionization processes in $C + O_2$ collisions in chapter V. This system was chosen because it was already known that charge

transfer processes in this particular case takes place into two channels, leading essentially to C^+ and C^- formation. We found however that in both channels also reactive ionization takes place, being even dominant over the simple charge transfer processes. Therefore it can be concluded that for these systems reactive ionization processes might be a non-negligible process in the first step of a chemical reaction.

CHAPTER I*

HYPERTHERMAL BEAMS SPUTTERED FROM ALKALIHALIDE SURFACES

Velocity selected beams of atoms and molecules have been produced by sputtering from various alkalihalide surfaces under 6 keV Ar^+ ion bombardment. The mass spectrum and the velocity distribution of these particles have been analyzed in the range from 0 - 13000m/s. In the low velocity part of the spectrum monatomic particles as well as polyatomic ones have been found. For velocities larger than 3000 m/s the number of sputtered molecules is very small compared to the number of atoms. In addition to typical sputtering velocity distributions, thermal distributions are also found, due to vaporization of the less effectively sputtered atoms from the crystals. Above a few eV the energy distribution of a given alkali or halogen atom is independent of the target from which it is sputtered. There are indications that some sputtered atoms and molecules are formed in long lived excited states.

1. INTRODUCTION

During the last years there has been a growing interest in "hot atom" beams for collision physics and chemistry, as well as for the investigation of surface phenomena. The supersonic gasflow method has an upper limit of about one eV kinetic energy, although by "seeding" energies can be obtained as high as 15 eV, dependent on the mass. The charge exchange method seems to work best above 10 eV. The sputtering method is especially suitable between 1 and 20 eV. Sputtering has been usually limited to the production of alkali beams, mainly because the detection of alkali atoms in the eV range is so easy by high temperature surface ionization. Only

* G.P. Können, J. Grosser, H. Haring, A.E. de Vries and J. Kistemaker, Rad.Eff., in press.

TABLE I

Values of various properties of alkalihalide crystals

	E_b (eV)[30]	E_d (eV)[31]	E_u (eV)[31]	R(Å)[31]	crystal type
LiCl		4.9	8.6	2.49	fcc NaCl type
NaCl	2.5	4.2	7.9	2.78	" "
KCl	2.4	4.4	7.2	3.14	" "
RbCl	2.3	4.4	7.0	3.28	" "
CsCl	2.0	4.6	6.6	3.48	prim.cubic CsCl type*
KBr	2.3	3.9	6.9	3.29	fcc NaCl type
CsBr	2.3	4.2	6.3	3.63	prim.cubic CsCl type
KI	2.3	3.3	6.5	3.53	fcc NaCl type
RbI		3.3	6.3	3.67	" "

* For temperatures above 728 K fcc NaCl type.

E_b is the binding energy of a molecule with respect to the surface, E_d the dissociation energy of the molecules in the gasphase, E_u the lattice energy and R the distance of the halogen ion to the nearest alkali ion in the crystal. The lattice energy is the energy required to separate the ions of a crystal to an infinite distance from each other. It is expressed in eV/ion pair.

recently scattering experiments were reported by Cohen, Young and Wexler [1] with Ba, Ti, Ta and Al beams, obtained by bombardment of Ba, Ti, Ta and Al targets with Ar^+ projectiles of 9 keV kinetic energy.

A very important category of projectiles for chemical research are the halogens and it is because of that reason that we have tried to develop sputtering of alkalihalide crystals (table I), and to investigate the detection possibilities for halogen atoms in the eV energy range [2].

Several investigators have studied certain aspects of the sputtering process of ionic crystals by heavy projectiles. Very few however, measured the neutral particles which usually represent the bulk of the sputtered material, the reason being that ions are much easier to detect [3-7].

Campbell and Cooper [8] looked for the neutral and charged sputtering products of:

$$KBr + Ar^+, Xe^+ \text{ (25 - 180 eV kinetic energy)},$$

but were only able to detect Br^-.

Stein [9] however, detected neutral K from (001) and (011) surfaces from:

$$KCl + Ne, Ar \text{ (400 eV kinetic energy)}.$$

He investigated the angular distribution of the sputtered products. Windawi and Cooper [10] recently measured the angular distribution of Cl from the (100) face of

$$KCl + Ar^+ \text{ (200 eV kinetic energy)}.$$

Navinšek [11] determined the total sputtering coefficient S for the (100) surface of many salts:

$$NaCl, KCl, KBr, LiF + Ar^+ \text{ (2 - 10 keV kinetic energy)}.$$

S proves to be 1.0 for NaCl, 1.9 for KCl, 0.6 for KBr and 2.2 for LiF at an Ar^+ kinetic energy of 10 keV. It is an important number for those people who want to use the sputtering process to generate hot atom beams for collision research.

Finally Schmidt-Bleek and Datz [12] sputtered AgI and AgBr surfaces by 0.5 - 7 keV Ar^+ ion beams and indeed got hot beams of Ag, I and

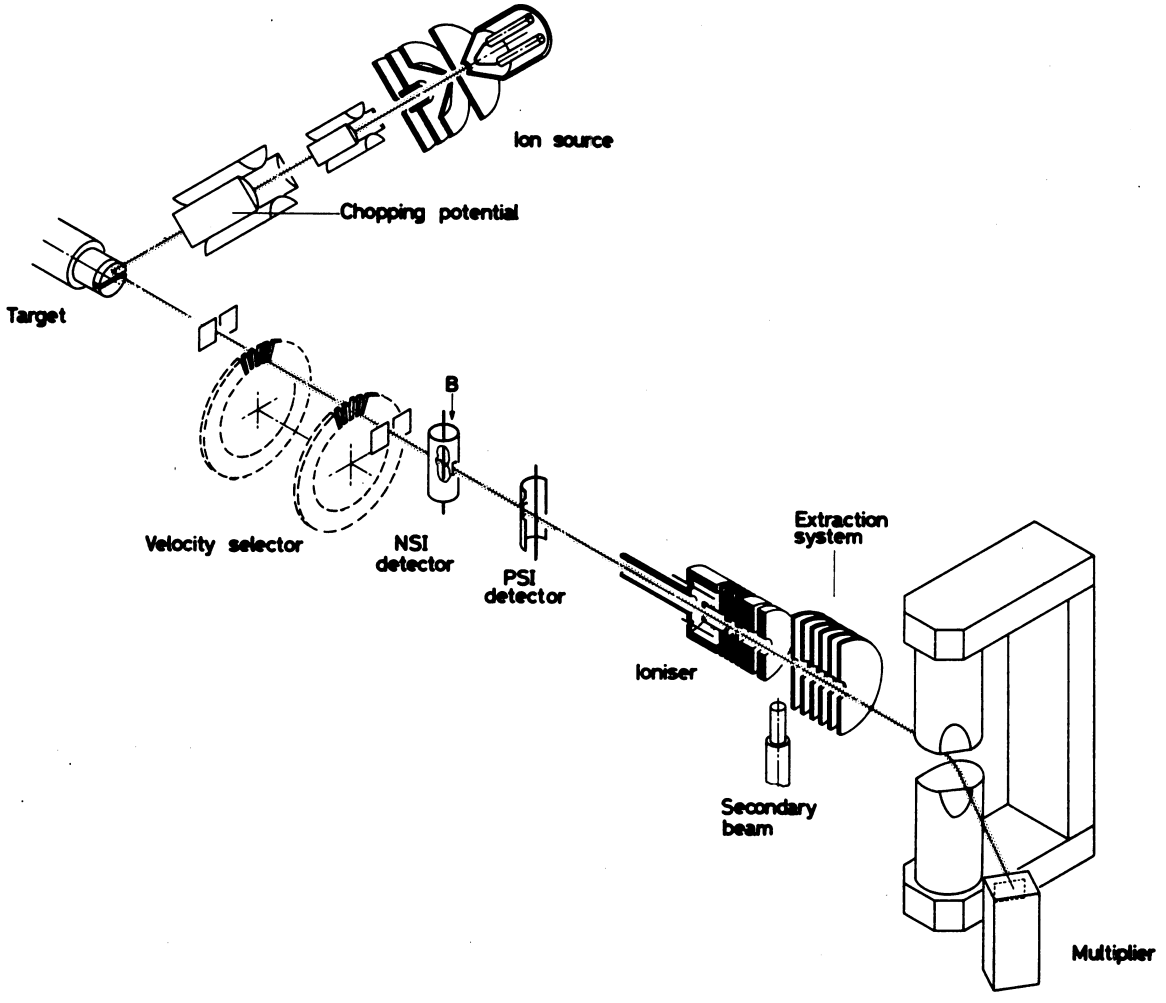

Fig. 1 - Schematic drawing of the apparatus. PSI and NSI stand for positive and negative surface ionization respectively.

Br atoms and of AgI and AgBr molecules.

In this paper we present the results of an analysis of mass spectra and velocity distributions of many atoms and radical groups sputtered from a large variety of ionic targets. Above about 2 to 4 eV this method seems to be suited for the production of well defined atom beams using a mechanical velocity selector. Below this energy the presence of dimers is confusing.

Apart from this application our investigations give information about the sputtering process from salt surfaces bombarded by a beam of 6 keV Ar^+ ions.

2. THE APPARATUS

2.1 General

A schematic view of the apparatus is seen in figure 1. Particles are sputtered from a target by a 6 keV Ar^+ ion beam. After collimating and velocity selection they can be detected on two hot wires by means of positive and negative surface ionization (PSI and NSI). The composition of the beam can be analyzed by means of a home made mass spectrometer ($\frac{m}{\Delta m} \simeq 20$) provided with an Extra Nuclear electron bombardment ionizer (efficiency 10^{-3} for thermal atoms). The four compartments containing the ion source, the velocity selector, the detection wires, and the mass spectrometer are differentially pumped, the first two compartments by oil diffusion pumps and the third and fourth by an ion getter pump and by two ion pumps respectively. Under working conditions the pressure is 10^{-5} torr in the first compartment, 10^{-7} in the second one and better than 10^{-7} in the third and fourth compartment.

2.2 Beam source

The ion source is the same one as used by Politiek et al. [13], who described it in detail. We put a chopping potential on one of the quadrupole lenses in order to modulate the sputtered beam. As targets various alkalihalide (MX) discs are used. They have been pressed at 5000 atm for about five minutes, and are about 2 mm thick. No

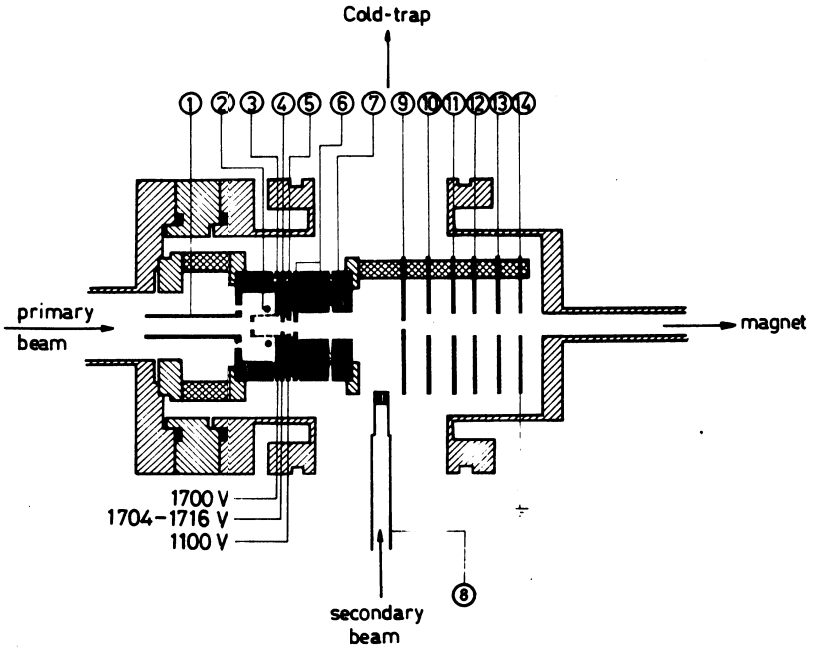

Fig. 2 - Scale drawing of the ionization system to make positive ions. Cylinder 1 prevents penetration of the outer fields; 2 filament; 3 ionization region; 4 extractor; 5, 6, 7 focusing lenses; the electric field from 7 to 12 is homogeneous; 12, 13, 14 form an Einzellens. The principal voltages are indicated.
Extractor 4 is used for discriminating thermal particles against hyperthermal ones at a voltage of + 1716 V. The surrounding house is at ground potential. The potential of cylinder 1 and of filament 2 is + 1600 V.

difficulties have been met in connection with possible charging up by the ion beam.

Possible sputtering products are halogen atoms X, alkali atoms M as well as different molecular species, and positive and negative ions. The positive ions, however, cannot leave the target holder, which has a potential of - 6 keV. The negative ions would get an energy of 6 keV. For such fast particles the transmission of the velocity selector is zero. Actually, even without velocity selection, we never found any negative ions in the mass spectrometer. We also tried sputtering from a Br_2 surface at liquid nitrogen temperature. Although this technique seems to give a larger amount of hyperthermal Br atoms than sputtering from a salt, it was not applied because it is technically more difficult. Furthermore, the large amount of Br_2 in the apparatus is a disadvantage.

2.3 Electron bombardment detector

A scale drawing of the ionizer and the additional lens system is shown in figure 2. In the lens system, the positive ions are accelerated with a potential difference of 1700 V, lenses 12, 13 and 14 are used as an Einzellens. It is possible to discriminate thermal background particles against hyperthermal ones, if one applies to lens 4 a potential which is positive with respect to that of the ionization region [14]. In our discrimination mode, particles with a kinetic energy higher than 4 eV are not attenuated, while the thermal background decreases by a factor of ten. The flow of the velocity selected beam of about 4.10^5 to 10^7 particles/s gave a mass spectrometer signal of 5 to 400 counts/s dependent on their velocity. Of course, for measurements of low energy sputtered particles this attenuation threshold has not been applied. Because of the large background signal (2.10^4 counts/s for I and 5.10^5 counts/s for Cl, if the attenuation threshold is not used), long measuring times were necessary to measure the velocity distributions.

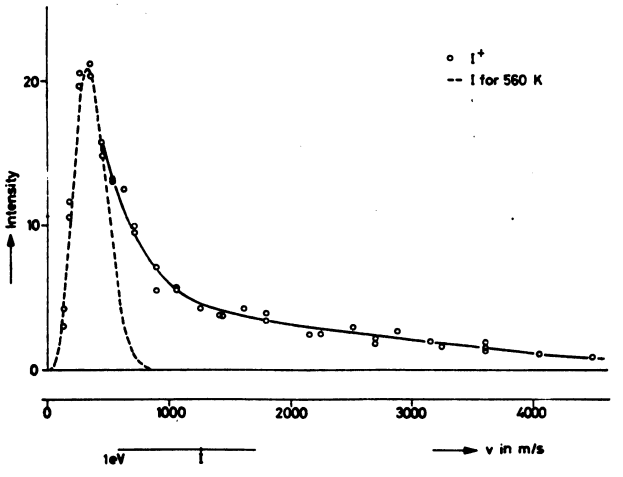

Fig. 3 - Flux distribution of I from KI in arbitrary units. The velocity at which the energy equals 1 eV is indicated. The calculated flux distribution of I atoms effusing from an oven at 560 K is indicated by the dashed line.

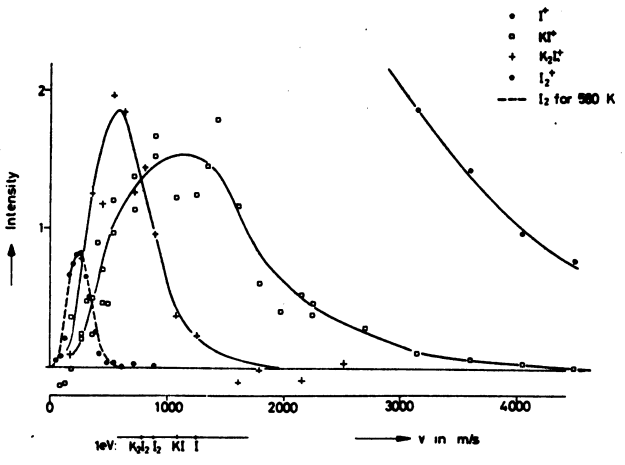

Fig. 4 - Flux distributions of the ions obtained from the neutral particles sputtered from KI. Same scale as in figure 3, arbitrary units. The I^+ distribution is the same as that in figure 3. The velocity at which the energy equals 1 eV is indicated for various particles. The calculated flux distribution of I_2 molecules effusing from an oven at 560 K is indicated by the dashed line and coincides with the I_2^+ measured distribution.

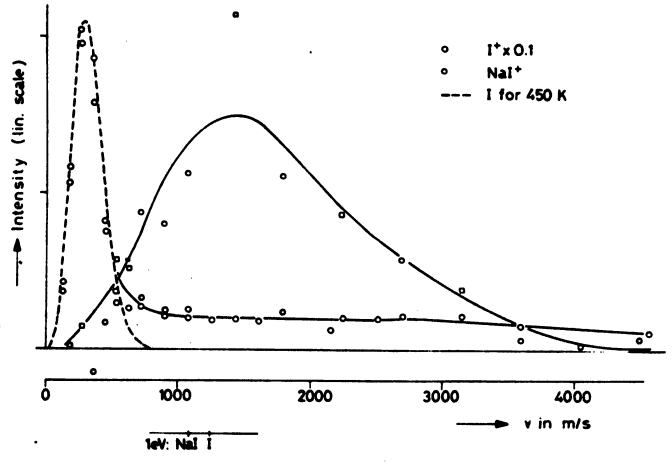

Fig. 5 - Flux distribution of I and NaI sputtered from NaI in arbitrary units. The velocity at which the energy equals 1 eV is indicated for the different particles. The calculated flux distribution of I atoms effusing from an oven at 450 K is indicated by the dashed line.

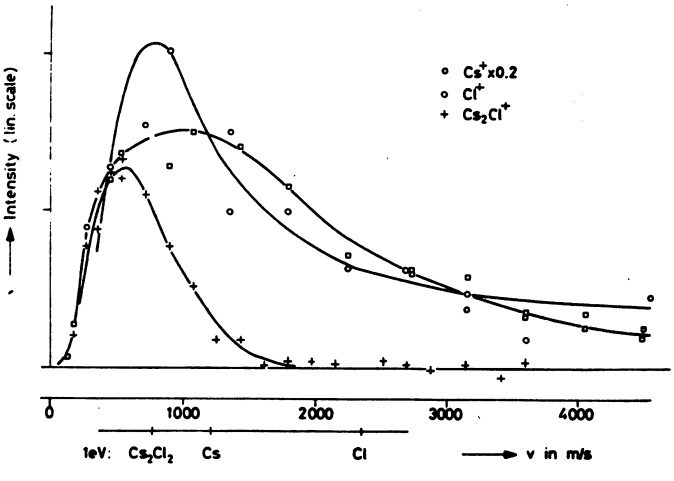

Fig. 6 - Flux distributions of ions obtained from the neutral particles sputtered from CsCl in arbitrary units. The velocity at which the energy equals 1 eV is indicated for various particles.

3. RESULTS AND DISCUSSION

3.1 Low velocity part of the spectrum

The velocity distributions up to 4000 m/s of particles sputtered from KI, NaI and CsCl are shown in figures 3 to 6. The curves give the signals obtained at the collector of the mass spectrometer. The ionization efficiency of the ionizer is inversely proportional to v; the velocity selector has a constant resolution $\Delta v/v$, and thus a transmission proportional to v. Therefore, the collector signal is proportional to the number of sputtered particles per velocity interval, $\frac{dS}{dv}(v)$. From this velocity distribution one easily obtains the energy distribution $\frac{dS}{dE}(E)$ of the products, using the relation

$$\frac{dS}{dE} = \frac{dS}{dv}\,\frac{dv}{dE} \propto \frac{1}{v}\,\frac{dS}{dv}\,, \tag{1}$$

in which E is the kinetic energy of the sputtered products.

In order to calculate from these curves the relative intensities of the neutrals, we have to know the mass spectra of these neutrals and the relative ionization cross sections for electron impact.

We found masses M^+, X^+, M_2^+, X_2^+, MX^+, M_2X^+, $M_3X_2^+$ and even higher mass numbers. Berkowitz and Chupka [15] who studied the mass spectra of MX vapors, conclude that the ions M^+, MX^+, M_2X^+ and $M_3X_2^+$ are formed by the processes

$$MX + e^- \nearrow \; MX^+ + 2e^- \tag{2}$$

$$\qquad\quad \searrow \; M^+ + X + 2e^- \tag{3}$$

$$M_nX_n + e^- \rightarrow M_nX_{n-1}^+ + X + 2e^- \; (n \geq 2) \tag{4}$$

so that the M_2X^+ peak, observed by us, is almost entirely due to M_2X_2 molecules. The X^+, M_2^+, X_2^+ and MX^+ peaks are mainly produced from the respective atoms and molecules. The M^+ peak is formed mainly from M atoms, but will also have a contribution from dissociative ionization of MX. The MX^+ peaks found in the mass spectra of CsCl and CsBr are small in comparison with those found with KI and NaI. This is in agreement with the measurements of Berkowitz and Chupka, who find that for KI and for NaI channels (2) and (3) have about the same cross section, while for CsCl and CsBr nearly all molecular ions dissociate. From these consideration we conclude the following. The velocity

distributions of the neutral X, X_2, MX and M_2X_2 particles are identical to the curves for X^+, X_2^+, MX^+ and M_2X^+ respectively, as given in figures 3, 4, 5 and 6. For alkali atoms this is only true at velocities for which the contribution from MX may be neglected.

The velocity distributions found can be divided into three groups. *First*, there are the atoms, which show a large intensity and are present in the beam to a measurable extent even at very high velocities. *Second*, we have the salt molecules MX and M_2X_2; they have somewhat lower intensity and go to zero much faster with velocity than the atom distributions do. An example of the *third* group is I_2. This molecule manifests itself only at low velocities.

Within the experimental error, the velocity distribution of I_2 which is shown in figure 4 is Maxwellian with a temperature of 560 K. The velocity distribution of I sputtered from KI shows a sharp maximum on the low velocity side, which can be fitted with a Maxwellian distribution of the same temperature of 560 K (figure 3). I sputtered from NaI also shows a sharp maximum on the low velocity side, which fits a Maxwellian distribution of 450 K (figure 5). Obviously, these low velocity atomic peaks belong to the third group of thermal particles. A possible explanation of the thermal peaks can be the fact that Na and K are sputtered more effectively than I under bombardment with Ar^+ ions. The sputtering ratio for a monatomic crystal depends on the energy transfer of the impinging particles, which is proportional to the factor

$$\frac{4m_1m_2}{(m_1+m_2)^2} \qquad (5)$$

where m_1 and m_2 are the masses of the bombarding particles and of the target atoms [16]. The same relation is expected to influence the ratio in which M and X atoms are removed from our crystals. We estimate from our ion beam intensity, using (5), that after a few milliseconds of sputtering, the upper layers of the crystal would mainly exist of I atoms if no vaporization would take place. The excess of I will vaporize thermally from the surface. If this is indeed the mechanism of production, the temperatures found are the temperatures of the surface locations from which the particles evaporate. A thermal peak should only arise for the atoms with the smaller sputter ratio. We measured thermal maxima in the velocity distributions of sputtered

alkalis from NaCl, CsCl, CsBr and CsI, under bombardment of Ar^+. In the case of NaF, KCl, KBr, KI, RbCl and RbI a thermal alkali peak was never observed. These measurements of the thermal alkali distributions were performed with the PSI detector. We have to mention that the height of the thermal peak is not stable, but depends strongly on the place from which sputtering takes place and on the time duration of the bombardment. For CsCl and CsBr for instance, the thermal Cs-peak sometimes vanishes totally. In figure 6 we clearly see only a higher energy distribution for the measured Cs^+ ions in the mass spectrometer.

In contrast to the molecules M_2 and X_2, the species MX and M_2X_2 are present at much higher energies than the thermal peaks. So we conclude that they are really a product of direct momentum transfer and not merely products of thermal vaporization.

In figure 7 the energy distributions $\frac{dS}{dE}(E)$ of K_2I_2, KI and I sputtered from KI are plotted on a double logarithmic scale. These energy distributions are calculated from the figures 3 and 4, using (1) and assuming that the K_2I^+, KI^+ and I^+ peaks in the mass spectrometer are entirely due to ionization of K_2I_2, KI and I respectively.

The energy distributions of the molecules go to zero much more rapidly than those of the atoms. The same is observed for the energy spectra of alkali dimers from polycrystalline alkali targets [17], and also for charged polyatomic clusters, sputtered from various polycrystalline metal targets [18,19,20].

The formation of dimers can be explained by a simple kinetic model. If a collision cascade arrives at the target surface there is a probability that two particles will leave the surface simultaneously. These particles will in general have different directions and velocities. If however the relative kinetic energy of these particles is lower than the potential energy between them, they will stick together and form a vibrational and rotational excited dimer. Dimers are likely to be formed mainly by sputtering of neighbouring particles, because they have the strongest interaction. One would expect that the formation of dimers decreases rapidly if they have kinetic energies above their dissociation energy. The formation of hyperthermal M_2 and X_2 dimers is unlikely, because the distance of equal particles in an alkalihalide lattice is larger than of unequal particles and their interaction in the gasphase is low. The fact that equal M or X ions in the lattice repel each other may also obstruct the formation of hyperthermal

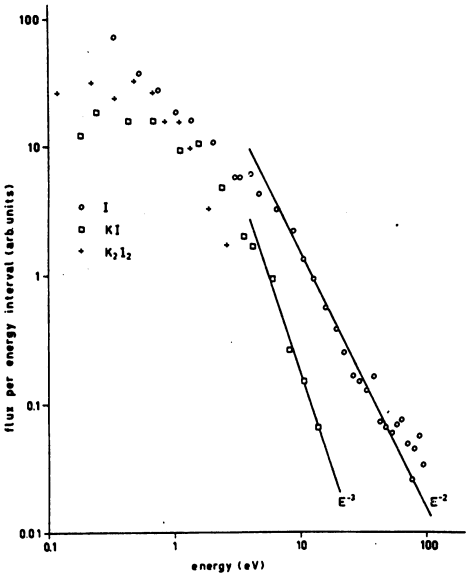

Fig. 7 - The energy distribution of K_2I_2, KI and I as a function of the kinetic energy.

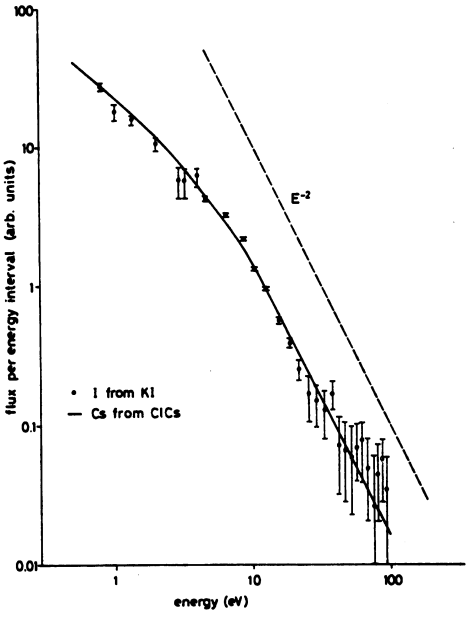

Fig. 8 - The energy distribution of I from a KI target bombarded with 6 keV Ar^+ ions. The solid line represents measurements of Cs from CsCl. The dashed line indicates a slope $\propto E^{-2}$.

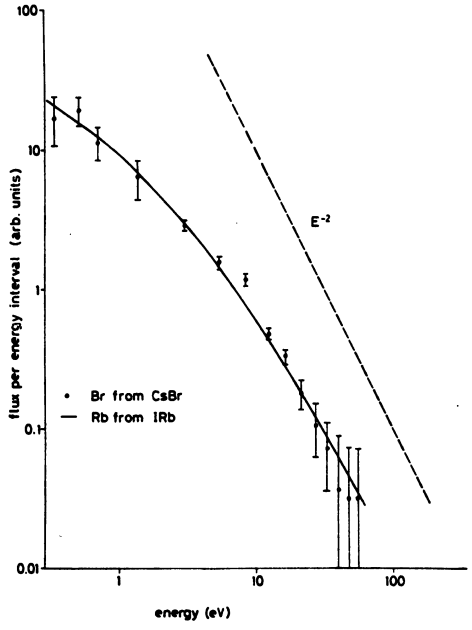

Fig. 9 - The energy distribution of Br from a CsBr target bombarded with 6 keV Ar^+ ions. The solid line represents measurements of Rb from RbI.
The dashed line indicates a slope $\propto E^{-2}$.

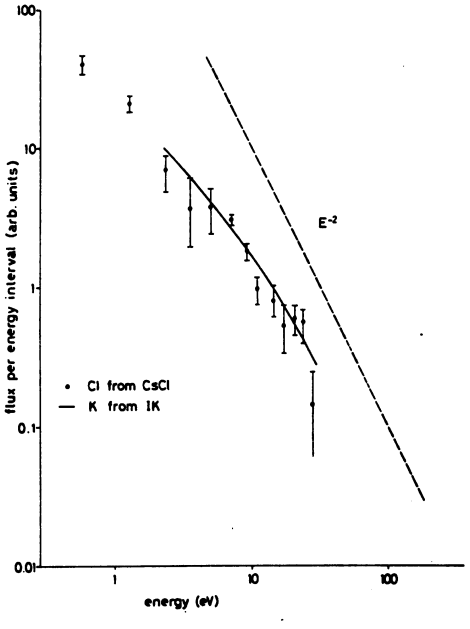

Fig. 10 - The energy distribution of Cl from a CsCl target bombarded with 6 keV Ar^+ ions. The solid line represents measurements of K from KI. The dashed line indicates a slope $\propto E^{-2}$.

M_2 and X_2 molecules.

Calculations on basis of this model give good agreement with the experimental energy distributions of the dimers [21]. The M_2X_2 molecules are likely to be formed in an analogous way.

3.2 High velocity spectrum

In figures 8, 9 and 10 we make a comparison of the energy distributions $\frac{dS}{dE}(E)$ for halogens and alkalis sputtered from targets with the same mass ratio, e.g. I from KI is compared with Cs from ClCs. The alkalis, for which a much higher precision is obtained, are represented by solid lines. They have been analyzed by means of the PSI detector with a Pt 8% W wire. The K fluxes have been corrected with the ionization efficiency values given by Politiek and Los [22], while those for Rb and Cs are uncorrected. The halogens were analyzed with the mass spectrometer. Their absolute intensities therefore cannot be compared directly with the intensities of the alkalis. By vertical shifting the alkali and halogen distributions can be made to coincide in each figure.

Measuring the chlorine component of LiCl, NaCl, KCl, RbCl and CsCl, by means of the NSI detector with a thoriated tungsten wire, we found above 3 eV the same energy distributions (see figure 11). The same was observed for bromine from CsBr and KBr. The energy distributions of the potassium component of K, KCl, KBr and KI measured with the PSI detector are also equal within a few percent for energies above 5 eV (see figure 12). Deviations below 5 eV may be partly due to PSI of MX and M_2X_2 molecules in the latter case.

The energy distributions of the atoms in figures 8, 9 and 10 tend towards E^{-2} as the energy increases. The latter distribution is to be expected from a random collision cascade model [23,24]. This model gives for the energy distribution of the particles outside the surface [23]

$$\frac{dS}{dE} \propto E(E+E_b)^{-3} \qquad (6)$$

in which E_b is the binding energy of an atom to the surface. Differentiating formula (6) one finds the maximum to occur at an energy of $\frac{1}{2}E_b$. The experimental curves reach a maximum below .5 eV, which is in agreement with the low binding energies E_b of .3 to .7 eV for adsorbed

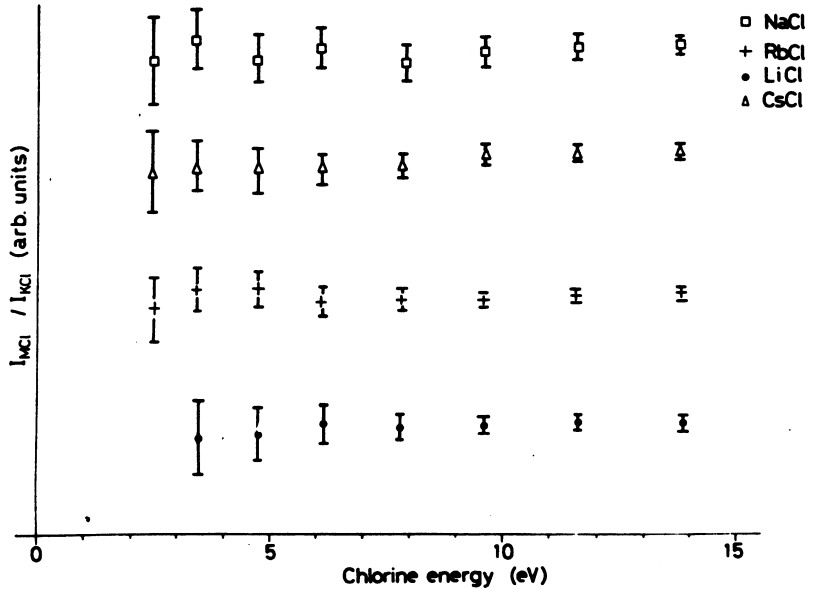

Fig. 11 - The NSI signal of beams sputtered from different chlorine containing targets MCl, divided by the signal from KCl, as a function of the chlorine kinetic energy.

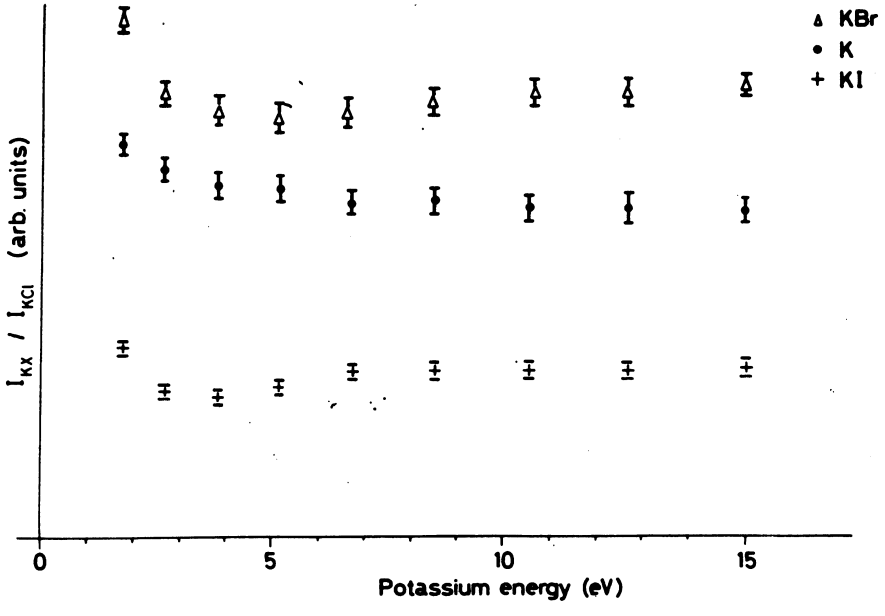

Fig. 12 - The PSI signal of beams sputtered from different potassium containing targets KX, divided by the signal of KCl, as a function of the potassium kinetic energy.

alkali and halogen atoms on alkalihalide surfaces [25,26].

The energy distributions of Rb, Br, K and Cl atoms in figures 9 and 10, being mutually equal within the experimental error, deviate slightly from E^{-2} even at higher energies. The value of the exponent is between -1.5 and -1.8 for energies above 10 eV. A similar deviation of the exponent has been reported in the energy distributions of the atoms sputtered from polycrystalline Au [27] and polycrystalline K [28]. The energy distributions of Cs and I in figure 8 show on the other hand a E^{-2} behaviour between 10 and 100 eV.

From figure 11 the most striking conclusion seems to be that Cl sputtered from LiCl, NaCl, KCl, RbCl and the heaviest salt CsCl seems to have exactly the same energy distribution, in spite of the fact that the energy distributions of for instance Cs and K from CsCl and KCl are different as can be seen from figures 8 and 10. The energy distribution of K also seems to be independent of the chemical composition of the target. A possible explanation for this effect might be that in the collision cascade the energy distribution of elements like K or Cl mixed with heavy or light elements like Cs, I or Li is hardly affected by the presence of the heavier or lighter particles. In fact, the transfer factor (5) indicates that a collision of K or Cl against an element like Cs, I or Li hardly leads to energy transfer. On the other hand, in a salt like KCl the masses of K and Cl are nearly equal which simply means that in a collision cascade for collision energies larger than say the binding energy in the lattice there will be no difference in the energy distribution functions of these particles. These facts combined with the low surface binding energy of adsorbed atoms apparently lead to equal energy dependences in the range above 5 eV.

From the data in figures 8, 9, 10, 11 and 12 one gets the impression that it is the energy distribution of the individual atoms in the collision cascades which determines the sputtering energy distributions. Indeed, the equal deviations from the E^{-2} behaviour of the energy distributions of K and Cl sputtered from various ionic targets as well as from the alkalimetal makes it unlikely that this is due to contributions like surface deflected recoils as is suggested for Au [27].

Moreover, the equality of the energy distributions of K and Cl and of I and Cs sputtered from KI and CsCl indicates that the crystal structure of the targets (being fcc NaCl type and prim.cubic CsCl

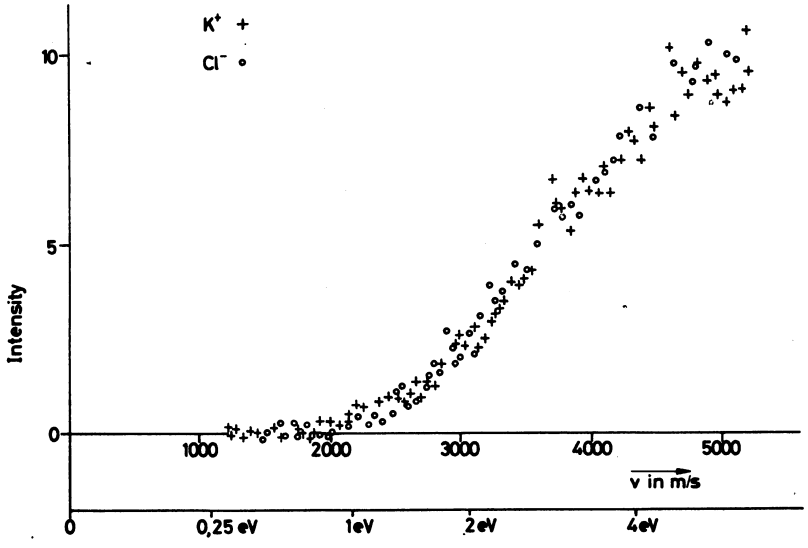

Fig. 13 - The K^+ and Cl^- signals arising from collisions of particles sputtered from a KCl crystal with a crossed beam of aniline molecules ($C_6H_5NH_2$) as a function of the sputtered beam velocity. The kinetic energy in the center of mass system of KCl and aniline has been indicated.

type respectively) does not play an important role. It is not impossible that the observed difference in the energy distributions for Cs and I with respect to K and Cl originates from inelastic processes in the collision cascades.

3.3 Metastable excited particles

Part of the sputtered products are in metastable states. Evidence for this was found for I and Br atoms and most of the MX molecules investigating the energy dependence for collisional ionization with heavy particles. *For the halogens*, this evidence was obtained from measurements on the process $X + C_6H_5NH_2 \rightarrow X^- + C_6H_5NH_2^+$ [29]. The thresholds for Br and I turned out to be smaller by about 0.4 and 0.9 eV than expected for the ground state atoms. These are just the excitation energies for the $^2P_{\frac{1}{2}}$ state of respectively Br and I. We estimate that about 30 to 50% of the sputtered halogen is formed in the $^2P_{\frac{1}{2}}$ state. This is found from a comparison of the experimental ionization cross sections for Br and I with the expected linear proportionality with the velocity near threshold. For Cl, the excitation energy of this state is only 0.1 eV, which is within the spread of the velocity selector. The measured threshold for ionization was in agreement with the expected one.

The conclusion that *metastable MX molecules* are present in the beam, comes from the following argument: We find M^+ and X^- ions if the sputtered beam is crossed with various secondary beams. Specific experiments were done by sputtering from KCl and CsCl targets with crossing beams of CH_4, C_6H_{12} (cyclohexane) and $C_6H_5NH_2$ molecules. The results for KCl on $C_6H_5NH_2$ are given in figure 13, those for CsCl are similar. These measurements have been performed below the threshold for the reaction $Cl + C_6H_5NH_2 \rightarrow Cl^- + C_6H_5NH_2^+$. The M^+ and X^- signals are equal for all velocities which fact is easiest understood if we assume that the process is taking place with the MX constituent of the beam. No sharp threshold has been found for these processes; they take place at center of mass energies as low as 0.3 eV. Since the energy for dissociation of ground state MX molecules into ground state M^+ and X^- ions is 5.1 eV for KCl and 4.9 eV for CsCl, we have to conclude that at least a fraction of the MX molecules is in an excited state. Nothing is known about the nature of this excitation. The M^+ and X^- signals are proportional to

exp(-a/v), within the experimental error (a is a constant). It is not clear if this exponential behaviour is caused by a collisional effect or if it is a time of flight effect related to the decay of the excited molecules into the ground state. In that case, the lifetime of these molecules would be 5.10^{-5} s.

REFERENCES

[1] R.B. Cohen, C.E. Young, S. Wexler, Chem.Phys.Letters 19 (1973) 99.

[2] G.P. Können, J. Grosser, A. Haring and A.E. de Vries, Chem.Phys.Letters 21 (1973) 445 (This thesis, chapter III).

[3] G.M. Batanov, Sov.Phys.Solid State 3 (1961) 471.
G.M. Batanov, Sov.Phys.Solid State 4 (1963) 1306.

[4] I.A. Abroyan, V.P. Lavrov, Sov.Phys.Solid State 4 (1963) 2382.

[5] I.A. Abroyan, V.P.Lavrov, I.G. Fedorova, Sov.Phys.Solid State 7 (1966) 2954.

[6] J.C. Kelly, M.C.E. Petersen, Phys.Letters 22 (1966) 295.

[7] Z. Jurela, Rad.Eff. 13 (1972) 167.

[8] A.B. Campbell, C.B. Cooper, J.Appl.Phys. 43 (1972) 863.

[9] R.P. Stein, Proc.Fifth Int.Conf on Ionization Phenomena in Gases, Munich, 1961 (North Holland Publ.Comp., Amsterdam 1962) Vol. 1, p. 118.

[10] H.M. Windawi, C.B. Cooper, Phys.Letters 43A (1973) 491.

[11] B. Navinšek, J.Appl.Phys. 36 (1965) 1678.

[12] F. Schmidt-Bleek, G. Ostrom, S. Datz, Rev.Sc.Instr. 40 (1969) 1351.

[13] J. Politiek, P.K. Rol, J. Los, P.G. Ikelaar, Rev.Sc.Instr. 39 (1968) 1147.

[14] E.K. Parks, C.E. Young, S. Wexler, Rev.Sc.Instr. 42 (1971) 1404.

[15] J. Berkowitz, W.A. Chupka, J.Chem.Phys. 29 (1958) 653.

[16] P.K. Rol, Thesis, University of Amsterdam, 1960.

[17] A.P.M. Baede, W.F. Jungman, J. Los, Physica 54 (1971) 459.

[18] Z. Jurela, B. Perović, Can.J.Phys. 46 (1968) 773.

[19] E. Dennis, R.J. MacDonald, Rad.Eff. 13 (1972) 243.

[20] G. Staudenmaier, Rad. Eff. 13 (1972) 87.

[21] G.P. Können, A. Tip, A.E. de Vries, to be pubished in Rad. Eff., (this thesis chapter II).

[22] J. Politiek, J. Los, Rev.Sci.Instr. 40 (1969) 1576.

[23] M.W. Thompson, Phil.Mag. 18 (1968) 377.

[24] P. Sigmund, Phys.Rev. 184 (1969) 383.

[25] I.G. Higginbotham, T.E. Gallon, M. Pruton, H. Tokutaka, Surface Sc. 21 (1970) 241.

[26] J.E. Hove, Phys.Rev. 99 (1955) 430.

[27] G.E. Chapman, B.W. Farmery, M.W. Thompson, I.H. Wilson, Rad.Eff. 13 (1972) 121.

[28] J. Politiek, J. Kistemaker, Rad.Eff. 2 (1969) 129.

[29] G.P. Können, J. Grosser, F. Eerkens, A. Haring, A.E. de Vries and J. Kistemaker, to be published. (this thesis chapter IV).

[30] Landolt-Börnstein, Zahlenwerte und Funktionen, Band I, teil 2, (Springer-Verlag, 1960).

[31] Handbook of Chemistry and Physics, 1972-1973.

CHAPTER II*

ON THE ENERGY DISTRIBUTION OF SPUTTERED CLUSTERS

A theoretical expression is obtained for the energy distribution of sputtered clusters from crystal surfaces. The derivation is based on a model where the atoms which constitute a cluster, are sputtered independently from the crystal according to their respective single particle energy distribution functions. Simultaneously sputtered atoms are then supposed to form a cluster if the sum of their initial relative kinetic energy and potential energy is less than the lowest dissociation energy of the cluster. A comparison with experimental results for $W_k (k \leq 3)$, K_2 and KI sputtered from polycrystalline W, K and KI surfaces respectively, shows good agreement. For the ionic crystal KI, evidence is obtained that sputtering of K and I atoms which are not closest neighbours gives an important contribution to dimer formation. The role of the binding energy E_b of the particles with respect to the surface is discussed.

1. INTRODUCTION

Although it is known for several years that sputtering results in the ejection of both monatomic and polyatomic particles, only in the last few years the energy distributions of some charged [1,2,3,4] and neutral [5,6,7] sputtered clusters have been reported.

A few attempts have been undertaken to explain the observed energy distributions of the sputtered clusters, which appear to be hypertherm-al and show a more rapid fall-off to zero than the monomer distributions. Joyes [8] calculated the mean energy of sputtered Cu_2 dimers, assuming that the dimer receives its energy from another Cu atom from

* Modified version of G.P. Können, A. Tip and A.E. de Vries, Rad.Eff., in press.

the target. Baede, Jungmann and Los [6] compared the energy distribution of K_2 dimers sputtered from polycrystalline K with a thermal spike theory. Staudenmaier [2] proposed a model in which the clusters are assumed to be formed from the individual atoms leaving the collision cascade, and in which the different binding energies of the various clusters with respect to the surfaces determine their ejection probabilities. In this paper we present a cluster sputtering model which assumes that all clusters are formed from recombination of simultaneously sputtered atoms. Assuming the initial energy distribution of these atoms to be independent of each other, we calculated the energy distribution for clusters from the monomer distributions. A comparison of the experimental data with this independent particle model shows that the model explains the observed energy distribution of dimers and trimers quite well.

2. THE MECHANISM OF CLUSTER SPUTTERING

In this section a precise formulation of the adopted mechanism for cluster formation is given. The basic assumptions are the following:

I - Particles belonging to a single collision cascade leave the surface at the same time t_o.

II - The constituent particles of a cluster originate from the same collision cascade. A set of k particles located at $x_1, x_2 \ldots x_k$ on the surface will form a cluster if at the initial time t_o the sum of the total potential energy $V(x_1 \ldots x_k)$ and the relative kinetic energy $\varepsilon^{(k)}$ of the k particles does not exceed the threshold for any dissociation channel of the cluster $\varepsilon^{(k)}_{diss}$:

$$\varepsilon^{(k)} + V(x_1 \ldots x_k) \leq \varepsilon^{(k)}_{diss} \tag{2.1}$$

III- The formation of clusters with more than k particles is excluded.

IV - Particles belonging to a certain collision cascade are initially uncorrelated. Thus the momentum distribution function of any k-particle cluster factorizes at time t_o into a product of one-particle functions.

In the following dS/dE denotes the probability density for a particle to be sputtered with energy E and angle θ with respect to the surface normal, dS/dv the probability density to be sputtered with velocity

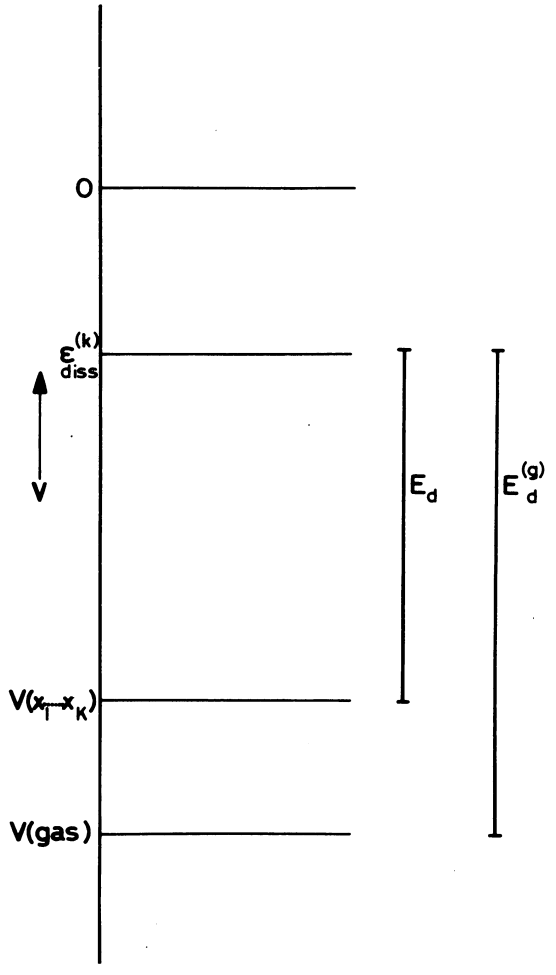

Fig. 1 - Schematic energy level diagram of a k-particle cluster. $\varepsilon_{diss}^{(k)}$ is the lowest dissociation energy of the cluster, V(gas) its potential energy in the gasphase and $V(x_1 \ldots x_k)$ the relative potential energy of its atoms at lattice places $x_1 \ldots x_k$. $E_d^{(g)}$ is its lowest dissociation energy in the gasphase, E_d at $x_1 \ldots x_k$.

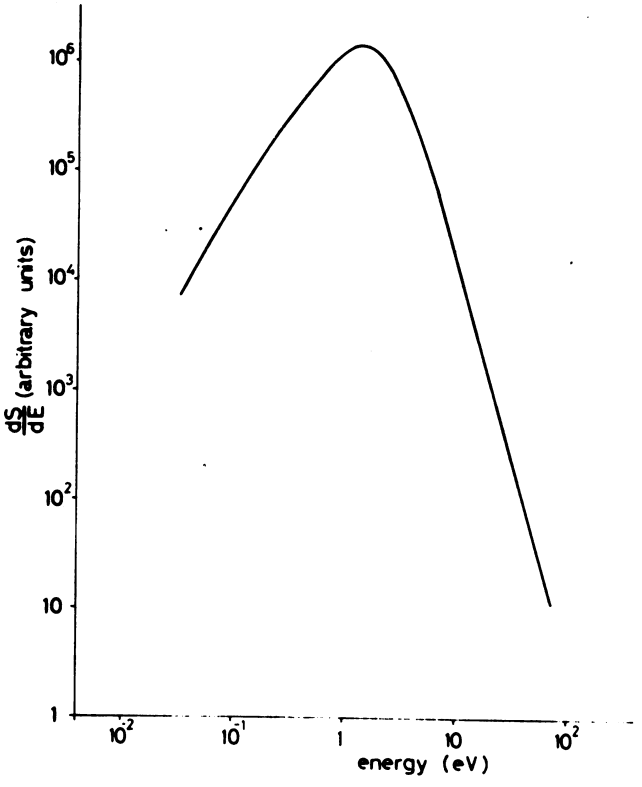

Fig. 2 - The energy distribution of dimers X_2, calculated from the atomic energy distribution with E_d = 1.0 eV, E_b = 0.5 eV and n = 1.5.

v and angle θ and $\phi(\underline{P})$ the probability density to be sputtered with momentum $\underline{P}$. The relation between these distributions is given by

$$\phi(\underline{P}) = M^{-1}P^{-2}\, dS/dv = M^{-1}P^{-1}\, dS/dE$$

$$(E = \tfrac{1}{2}Mv^2,\ \underline{P} = M\underline{v}) \qquad (2.2)$$

where M is the mass of the sputtered particle. In order to perform numerical calculations, an additional assumption will be made:

V - The initial one particle energy and angle distribution functions mentioned under IV are of the form

$$dS/dE = C_j\, E(E + E_b^{(j)})^{-(n_j+1)} f_j(\theta) \qquad (2.3)$$

where $E_b^{(j)}$ is the binding energy of an atom of species j with respect to the surface, n_j is a constant, C_j a normalization factor and $f_j(\theta)$ the angular distribution of the sputtered atoms. Formula (2.3) is obtained from the assumption that in the collision cascade the energy distribution dS/dE of atom j is proportional to E^{-n_j} [9,10].

In many cases condition (2.1) excludes the formation of a k particle cluster if these k particles are initially not neighbours. This is due to the circumstance that usually $V(x_1 \ldots x_k)$ is close to zero for such a set of particles, whereas $\varepsilon^{(k)}$ is always positive and $\varepsilon_{diss}^{(k)} \leq 0$. If on the other hand the particles are neighbours, then for small clusters it often makes sense to approximate $E_d = \varepsilon_{diss}^{(k)} - V(x_1 \ldots x_k)$ by the lowest dissociation energy $E_d^{(g)}$ of the cluster in the gasphase. In general however $E_d \leq E_d^{(g)}$. Thus condition (2.1) can be rewritten as

$$\varepsilon^{(k)} \leq E_d \leq E_d^{(g)} \qquad (2.4)$$

The transition of formula (2.1) to (2.4) is illustrated schematically in figure 1. Here V(gas) is the potential energy of the ground state cluster in the gasphase.

The above assumptions allow the calculation of the energy and angle dependence of cluster distribution functions for any $f_j(\theta)$. The asymptotic behaviour of this function for a k_1+k_2 particle cluster $X_{k_1}Y_{k_2}$ for E tending to infinity is then found to be (see section 3)

$$dS/dE \propto E^{-k_1n_1-k_2n_2-0.5(k_1+k_2-1)} f_1^{k_1}(\theta)\, f_2^{k_2}(\theta) \qquad (2.5)$$

For $f_j(\theta) = \cos\theta$, the velocity distribution of dimers in the normal direction becomes

$$dS/dv = 2\pi N_1 N_2 (m_1+m_2)^3 \, v^2 \int_0^{(2\mu E_d)^{\frac{1}{2}}} d\zeta . \zeta^2 \int_{-\min(1,m_1 v/\zeta)}^{\min(1,m_2 v/\zeta)} dz (m_1 v+\zeta z)(m_2 v-\zeta z) .$$

$$[m_1^2 v^2+\zeta^2+2m_1 v\zeta z+2m_1 E_b^{(1)}]^{-(n_1+1)} [m_2^2 v^2+\zeta^2-2m_2 v\zeta z+2m_2 E_b^{(2)}]^{-(n_2+1)} \qquad (2.6)$$

in which m_1 and m_2 are the masses of particles 1 and 2, μ their reduced mass, and N_1 and N_2 the normalization constants of the monomer momentum distributions. From this one obtains the energy distribution dS/dE through the relation (2.2). For dimers dS/dE behaves as follows: it starts like E^2, passes through a maximum, falls off to zero at high energies as $E^{-n_1-n_2-0.5}$, which is indeed much more rapidly than the energy distributions of the monomers. The behaviour of this function is illustrated in figure 2 on a log-log plot for a homonuclear dimer X_2 with E_d = 1.0 eV, E_b = 0.5 eV and n = 1.5. It is not possible to obtain a better than order of magnitude estimate for the ratio of monomers and dimers at a given energy and in a given direction. For this, specific knowledge is needed about the statistics of the occurence of the various possible configurations at the surface of particles to be sputtered.

3. CALCULATION OF CLUSTER DISTRIBUTION FUNCTIONS

In this section, first the expression for the distribution function $\phi_{12}(\underline{P})$ of a cluster of k particles is derived from the momentum distributions $\phi_1(\underline{P})$ and $\phi_2(\underline{P})$ of two subclusters. Then, the dimer distribution function $\phi^{(2)}(\underline{P})$ is derived and its asymptotic behaviour is studied. Finally the model is applied to higher clusters, and an expression is given for the high energy asymptote of their energy distribution functions.

3.1 The distribution function

According to the model put forward in the previous section, the calculation of the cluster distribution function amounts to a calculation of the available phase-space under condition (2.4). The normalized probability density for two subclusters to have relative energy ε_{12} and centre-of-mass momentum $\underline{P}$ is given by

$$\phi_{12}(\varepsilon_{12},\underline{P}) = \int d\underline{p}_1 \int d\underline{p}_2 \phi_1(\underline{p}_1)\phi_2(\underline{p}_2)\delta(\varepsilon_{12}-E_{rel})\delta(\underline{P}-\underline{P}_{cm}) \qquad (3.1.1)$$

Here is $\underline{p}_j$ the momentum vector of subcluster j, and $\phi_j(\underline{p}_j)$ is the normalized momentum distribution function for sputtered subcluster of species j. The relative energy E_{rel} is given by

$$E_{rel} = \tfrac{1}{2}\mu(\underline{p}_1/m_1-\underline{p}_2/m_2)^2, \qquad (3.1.2)$$

where m_j is the mass of a particle of subcluster j, and $\mu = m_1m_2/(m_1+m_2)$.

After a change to centre-of-mass and relative variables according to

$$\underline{P}_{cm} = \underline{p}_1+\underline{p}_2, \quad \underline{p} = \mu(\underline{p}_1/m_1-\underline{p}_2/m_2), \qquad (3.1.3)$$

$\phi_{12}(\varepsilon_{12},\underline{P})$ can be written as

$$\phi_{12}(\varepsilon_{12},\underline{P}) = \int d\underline{P}_{cm} \int d\underline{p}\ \phi_1((m_1/M)\underline{P}_{cm}+\underline{p})\phi_2((m_2/M)\underline{P}_{cm}-\underline{p}).$$

$$.\delta(\varepsilon_{12}-p^2/2\mu)\ \delta(\underline{P}_{cm}-\underline{P}) = 2\mu \int d\underline{p}\ \phi_1(q_1\underline{P}+\underline{p})\phi_2(q_2\underline{P}-\underline{p}).\delta(p^2-2\mu\varepsilon_{12})$$

where $M = m_1+m_2$ and $q_j = m_j/M$. The remaining δ-function can be removed by means of the identity

$$\delta(p^2-2\mu\varepsilon_{12}) = \tfrac{1}{2}(2\mu\varepsilon_{12})^{-\frac{1}{2}}\{\delta(p-(2\mu\varepsilon_{12})^{\frac{1}{2}})+\delta(p+(2\mu\varepsilon_{12})^{\frac{1}{2}})\} \qquad (3.1.4)$$

To achieve this $\underline{p}$ is written as $\underline{p} = p\underline{u}$, $\underline{u}$ being the unit vector along $\underline{p}$. Then $d\underline{p} = p^2\,dp\,d\underline{u}$, $d\underline{u}$ indicating an integration over a solid angle, and

$$\phi_{12}(\varepsilon_{12},\underline{P}) = 2\mu \int_0^\infty dp\cdot p^2 \int d\underline{u}\ \phi_1(q_1\underline{P}+p\underline{u})\ \phi_2(q_2\underline{P}-p\underline{u}).\tfrac{1}{2}\zeta^{-1}\{\delta(p-\zeta)+\delta(p+\zeta)\}$$

$$= \mu\zeta \int d\underline{u}\ \phi_1(q_1\underline{P}+\zeta\underline{u})\ \phi_2(q_2\underline{P}-\zeta\underline{u}) \qquad (3.1.5)$$

with $$\zeta = (2\mu\varepsilon_{12})^{\frac{1}{2}} \qquad (3.1.6)$$

From this the normalized cluster distribution function $\phi_{12}(\underline{P})$ is obtained by integration over ε_{12} from zero under condition (2.4):

$$\phi_{12}(\underline{P}) = \int_0^\infty d\varepsilon_{12}\ \phi_{12}(\varepsilon_{12},\underline{P})\ h(E_d-\varepsilon_{12}) \tag{3.1.7}$$

where the Heaviside step function $h(E_d-\varepsilon_{12})$ ($h(x) = 0$, $x < 0$ and $h(x) = 1$, $x \geq 0$) fixes ε_{12} in the bounded interval $[0,E_d]$. Thus the normalized probability density is given by

$$\phi_{12}(\underline{P}) = \int_0^{E_d} d\varepsilon_{12}\ \phi_{12}(\varepsilon_{12},\underline{P}) = \int_0^{(2\mu E_d)^{\frac{1}{2}}} \zeta^2 d\zeta \int d\underline{u}\ \phi_1(q_1\underline{P}+\zeta\underline{u})\phi_2(q_2\underline{P}-\zeta\underline{u}) \tag{3.1.8}$$

3.2 The dimer distribution function

Formula (3.1.8) enables a straightforward calculation of the dimer distribution function $\phi^{(2)}(\underline{P})$. For this the angle and energy distribution of the monomers is taken to be of the form given by (2.3) with $f_j(\theta) = \cos\theta$ for both atoms of the dimer. From (2.1) the following normalized momentum distribution $\phi_j^{(1)}(\underline{p}_j)$ of species j is obtained:

$$\phi_j^{(1)}(\underline{p}_j) = N_j(\underline{p}_j\cdot\underline{e})\ h((\underline{p}_j\cdot e))\cdot(p_j^2+L_j)^{-(n_j+1)} \tag{3.2.1}$$

Here is $\underline{e}$ the unit vector normal to the surface,

$$N_j = 2n_j(n_j-1)L_j^{n_j-1}/\pi,\quad L_j = 2m_j\ E_b^{(j)} \tag{3.2.2}$$

The Heaviside step function $h((\underline{p}_j\cdot\underline{e}))$ takes into account that sputtering only takes place in one half space. Since $\phi^{(2)}(\underline{P})$ is symmetric about $\underline{e}$, $\underline{P}$ can be fixed in the YZ-plane in a coordinate system with $\underline{e}$ along the positive Z-axis. The angle between $\underline{P}$ and $\underline{e}$ is θ. Let the polar angles of $\underline{u}$ be ϑ and ψ, so that

$$\underline{P}\cdot\underline{e} = P\cos\theta \quad \underline{P}\cdot\underline{u} = P(\sin\theta\sin\vartheta\sin\psi+\cos\vartheta\cos\theta)$$

$$\underline{u}\cdot\underline{e} = \cos\vartheta \quad d\underline{u} = \sin\vartheta d\vartheta d\psi \tag{3.2.3}$$

Then formula (3.1.8) becomes

$$\phi^{(2)}(\underline{P}) = \phi^{(2)}(P,\theta) = N_1 N_2 \int_0^{(2\mu E_d)^{\frac{1}{2}}} d\zeta\cdot\zeta^2 \int_0^{2\pi} d\psi \cdot \int_0^{\pi} d\vartheta\cdot \sin\vartheta \cdot$$

$$\cdot(q_1 P\cos\theta+\zeta\cos\vartheta)\; h(q_1 P\cos\theta+\zeta\cos\vartheta)\cdot$$
$$\cdot(q_2 P\cos\theta-\zeta\cos\vartheta)\; h(q_2 P\cos\theta-\zeta\cos\vartheta)\cdot$$
$$\cdot[q_1^2P^2+\zeta^2+2q_1P\zeta(\sin\theta\sin\vartheta\sin\psi+\cos\theta\cos\vartheta)+L_1]^{-(n_1+1)}$$
$$\cdot[q_2^2P^2+\zeta^2-2q_2P\zeta(\sin\theta\sin\vartheta\sin\psi+\cos\theta\cos\vartheta)+L_2]^{-(n_2+1)}.$$

It is convenient to change from ϑ to $z = \cos\vartheta$. Then the Heaviside functions can be replaced by a condition on the integration interval for z:

$$\phi^{(2)}(P,\theta) = N_1 N_2 \int_0^{(2\mu E_d)^{\frac{1}{2}}} d\zeta\cdot\zeta^2 \int_0^{2\pi} d\psi \int_{-\min(1,q_1P\cos\theta/\zeta)}^{+\min(1,q_2P\cos\theta/\zeta)} dz$$

$$\cdot(q_1 P\cos\theta+\zeta z)(q_2 P\cos\theta-\zeta z)$$
$$\cdot[q_1^2P^2+\zeta^2+2q_1P\zeta\{\sin\theta(1-z^2)^{\frac{1}{2}}\sin\psi+z\cos\theta\}+L_1]^{-(n_1+1)}$$
$$\cdot[q_2^2P^2+\zeta^2-2q_2P\zeta\{\sin\theta(1-z^2)^{\frac{1}{2}}\sin\psi+z\cos\theta\}+L_2]^{-(n_2+1)} \qquad (3.2.4)$$

This is the final expression for the distribution function of sputtered dimers. For the case $\theta = 0$, i.e. sputtering of dimers in the direction normal to the surface it simplifies significantly:

$$\phi^{(2)}(P,0) = 2\pi\, N_1 N_2 \int_0^{(2\mu E_d)^{\frac{1}{2}}} d\zeta\cdot\zeta^2 \int_{-\min(1,q_1P/\zeta)}^{+\min(1,q_2P/\zeta)} dz$$
$$\cdot(q_1P+\zeta z)(q_2P-\zeta z)[q_1^2P^2+\zeta^2+2q_1P\zeta z+L_1]^{-(n_1+1)}$$
$$[q_2^2P^2+\zeta^2-2q_2P\zeta z+L_2]^{-(n_2+1)} \qquad (3.2.5)$$

From this the velocity distribution dS/dv of sputtered dimers in the normal direction (formula 2.6) can be calculated with (2.2). In section 4 the results of numerical calculations of this expression are given and compared with experimental data on dimer sputtering.

3.3 Asymptotic behaviour of dimers

It is not difficult to obtain from (3.2.4) the behaviour of $\phi^{(2)}(P,\theta)$ for P tending to infinity and zero, respectively. In the first case it is even more convenient to turn to the expression (3.1.8) for $\phi^{(2)}(\underline{P})$. For large absolute values of $\underline{P}$ the term $\zeta\underline{u}$ in the argument of ϕ_j can be neglected, since ζ ranges through the bounded interval $[0,(2\mu E_d)^{\frac{1}{2}}]$. Thus, for P tending to infinity:

$$\phi^{(2)}(P,\theta) \sim \int_0^{(2\mu E_d)^{\frac{1}{2}}} d\zeta\cdot\zeta^2 \int d\underline{u}\ \phi_1^{(1)}(q_1\underline{P})\ \phi_2^{(1)}(q_2\underline{P})$$

$$\sim (4\pi/3)\cdot N_1N_2\cdot q_1^{-(2n_1+1)} q_2^{-(2n_2+1)}\cdot(2\mu E_d)^{3/2}\cdot$$

$$\cdot P^{-2(n_1+n_2+1)}\cos^2\theta \qquad (3.3.1)$$

The behaviour of $\phi^{(2)}(P,\theta)$ for P tending to zero is obtained in the following way. It is convenient to split $\phi^{(2)}(P,\theta)$ into four parts and to consider each part separately. Thus for $\theta < \pi/2$:

$$\phi^{(2)}(P,\theta) = \int_0^{q_2P\cos\theta} d\zeta \int_0^1 dz\ldots + \int_{q_2P\cos\theta}^{(2\mu E_d)^{\frac{1}{2}}} d\zeta \int_0^{q_2P\cos\theta/\zeta} dz\ \ldots. +$$

$$+ \int_0^{q_1P\cos\theta} d\zeta \int_{-1}^{0} dz\ldots + \int_{q_1P\cos\theta}^{(2\mu E_d)^{\frac{1}{2}}} d\zeta \int_{-q_1P\cos\theta/\zeta}^{0} dz\ \ldots. = \sum_{j=1}^{4}\phi_j^{(2)}(P,\theta)$$

(3.3.2)

For small P the terms L_1 and L_2 in the denominator become the leading terms in $\phi_1^{(2)}(P,\theta)$ and $\phi_3^{(2)}(P,\theta)$ so that

$$\phi_1^{(2)}(P,\theta) \sim 2\pi\ N_1N_2\ L_1^{-(n_1+1)}\ L_2^{-(n_2+1)} \int_0^{q_2P\cos\theta} d\zeta\cdot\zeta^2\ \cdot$$

$$\cdot \int_0^1 dz\ (q_1P\cos\theta+\zeta z)(q_2P\cos\theta-\zeta z) =$$

$$= 2\pi\ N_1N_2[(5/24)q_1q_2^4 + (7/120)q_2^5]\ L_1^{-(n_1+1)}L_2^{-(n_2+1)}(P\cos\theta)^5 \qquad (3.3.3)$$

By interchanging the subscripts 1 and 2 the corresponding expression for $\phi_3^{(2)}(P,\theta)$ is obtained. In $\phi_2^{(2)}(P,\theta)$ and $\phi_4^{(2)}(P,\theta)$ the leading term in the denominator is $[\zeta^2+L_1]^{-(n_1+1)}\,[\zeta^2+L_2]^{-(n_2+1)}$ since now ζ ranges up to $(2\mu E_d)^{\frac{1}{2}}$, instead of $q_jP\cos\theta$, $j = 1,2$ in the former case. Thus, for P tending to zero:

$$\phi_2^{(2)}(P,\theta) \sim 2\pi\, N_1N_2 \int_{q_2P\cos\theta}^{(2\mu E_d)^{\frac{1}{2}}} d\zeta\cdot\zeta^2 \int_o^{q_2P\cos\theta/\zeta} dz\;\; (q_1P\cos\theta+\zeta z)(q_2P\cos\theta-\zeta z)\cdot$$

$$\cdot[\zeta^2+L_1]^{-(n_1+1)}\,[\zeta^2+L_2]^{-(n_2+1)} \sim$$

$$\sim 2\pi\, N_1N_2(\tfrac{1}{2}q_1q_2^2+1/6q_2^3) \int_o^{(2\mu E_d)^{\frac{1}{2}}} d\zeta\cdot\zeta[\zeta^2+L_1]^{-(n_1+1)}[\zeta^2+L_2]^{-(n_2+1)}\cdot$$

$$\cdot P^3\cos^3\theta, \qquad (3.3.4)$$

and the corresponding expression for $\phi_4^{(2)}(P,\theta)$ is obtained by interchanging the subscripts 1 and 2. Comparing the result with (3.3.3) it is seen that $\phi_2^{(2)}(P,\theta)$ and $\phi_4^{(2)}(P,\theta)$ are the leading terms for P tending to zero. Hence, for P tending to zero:

$$\phi^{(2)}(P,\theta) \sim 2\pi\, N_1N_2(\tfrac{1}{2}q_1q_2^2+\tfrac{1}{2}q_1^2q_2+1/6q_1^3+1/6q_2^3)\cdot$$

$$\cdot \int_o^{(2\mu E_d)^{\frac{1}{2}}} d\zeta\cdot\zeta\,[\zeta^2+L_1]^{-(n_1+1)}[\zeta^2+L_2]^{-(n_2+1)}P^3\cos^3\theta \qquad (3.3.5)$$

3.4 High energy distribution function for a k-particle cluster

The formalism developed in section 3.1 allows the calculation of the distribution function of a k-particle cluster. In order to do so, we consider the cluster to be built up from two subclusters 1 and 2. We introduce the subcluster distribution function $\phi_j(\underline{p}_j,\varepsilon_j)$, where ε_j is the relative kinetic energy of the particles in subcluster j at the time t_o at which the subcluster leaves the surface, and $\underline{p}_j$ its centre of mass momentum. For the clusterdistribution $\phi_{12}(\underline{P},\varepsilon_{12},\varepsilon_1,\varepsilon_2)$ a similar formula can be derived as for $\phi_{12}(\underline{P},\varepsilon_{12})$ in section 3.1, formula (3.1.5):

$$\phi_{12}(\underline{P},\varepsilon_{12},\varepsilon_1,\varepsilon_2) = \mu\zeta\int d\underline{u}\ \phi_1(q_1\underline{P}+\zeta\underline{u},\varepsilon_1)\ \phi_2(q_2\underline{P}-\zeta\underline{u},\varepsilon_2) \qquad (3.4.1)$$

Clearly, $\varepsilon_{12}+\varepsilon_1+\varepsilon_2$ represents the total internal kinetic energy $\varepsilon^{(k)}$ of the atoms in the cluster at time t_o. The bound cluster distribution function $\phi_{12}(\underline{P})$ is found by integration over ε_{12}, ε_1 and ε_2 under condition (2.4):

$$\phi_{12}(\underline{P}) = \int_0^\infty\cdots\int_0^\infty d\varepsilon_{12}d\varepsilon_1 d\varepsilon_2\ \phi_{12}(\underline{P},\varepsilon_{12},\varepsilon_1,\varepsilon_2)\ h(E_d-\varepsilon_{12}-\varepsilon_1-\varepsilon_2) \qquad (3.4.2)$$

in which the Heaviside function $h(E_d-\varepsilon_{12}-\varepsilon_1-\varepsilon_2)$ takes into account that the initial internal kinetic energy never exceeds the dissociation energy E_d of the cluster. It can be proved [11] that (3.4.2) is independent of the choice of subclusters 1 and 2. Therefore these formula allow the calculation of any clusterdistribution function, starting with the monomer distribution functions $\phi_j^{(1)}(\underline{p}_j)$.

For the high energy asymptote of the cluster distribution function, the term $\zeta\underline{u}$ in (3.4.1) can be neglected. This is due to the fact that in (3.4.2) ζ ranges through the bounded interval $[0,(2\mu E_d)^{\frac{1}{2}}]$ due to condition (2.4) and because ε_j is bounded from below ($\varepsilon_j \geq 0$). Thus, for $\underline{P}$ tending to infinity

$$\phi_{12}(\underline{P},\varepsilon_{12},\varepsilon_1,\varepsilon_2) \sim \mu\zeta\int d\underline{u}\ \phi_1(q_1\underline{P},\varepsilon_1)\ \phi_2(q_2\underline{P},\varepsilon_2)$$

$$\propto \varepsilon_{12}^{\frac{1}{2}}\ \phi_1(q_1\underline{P},\varepsilon_1)\ \phi_2(q_2\underline{P},\varepsilon_2) \qquad (3.4.3)$$

Formulae (3.4.3) and (3.4.2) are convenient starting points for the study of the behaviour of the k-particle cluster distribution $\phi^{(k)}(\underline{P})$ at high energies, starting with monomer distributions $\phi^{(1)}(\underline{p})$. This will be done explicitly for homonuclear k-particle clusters X_k the generalization to different situations is obvious.

For the construction of a k-particle cluster distribution function from the monomer distribution function, we define the parameter $\varepsilon_{1,k-1}$, being the relative kinetic energy of particle k and the subcluster consisting of all k-1 subsequent particles. Then, for dimers X_2 formula (3.4.3) becomes

$$\phi^{(2)}(\underline{P},\varepsilon_{1,1}) \propto \varepsilon_{1,1}^{\frac{1}{2}}\ \phi^{(1)}(\tfrac{1}{2}\underline{P})\ \phi^{(1)}(\tfrac{1}{2}\underline{P}) = \varepsilon_{1,1}^{\frac{1}{2}}[\phi^{(1)}(\tfrac{1}{2}\underline{P})]^2 \qquad (3.4.4)$$

For trimers, one finds

$$\phi^{(3)}(\underline{P},\varepsilon_{1,1},\varepsilon_{1,2}) \propto \varepsilon_{1,2}^{\frac{1}{2}}\ \phi^{(1)}(1/3\underline{P})\ \phi^{(2)}(2/3\underline{P})$$

$$\propto \varepsilon_{1,1}^{\frac{1}{2}}\varepsilon_{1,2}^{\frac{1}{2}}[\phi^{(1)}(1/3\underline{P})]^3 \qquad (3.4.5)$$

and so on. In a similar way, for a k-particle cluster

$$\phi^{(k)}(\underline{P},\varepsilon_{1,1}\cdots\varepsilon_{1,k-1}) \propto \{\prod_{x=1}^{k-1}\varepsilon_{1,x}^{\frac{1}{2}}\}.[\phi^{(1)}(\underline{P}/k)]^k \qquad (3.4.6)$$

Here, $\sum_{x=1}^{k-1}\varepsilon_{1,x}$ is the internal kinetic energy $\varepsilon^{(k)}$ of the cluster at t_o. Integration over all $\varepsilon_{1,k-1}$ yields the distribution function $\phi^{(k)}(\underline{P})$. Since $\phi^{(k)}(\underline{P},\varepsilon_{1,1}\cdots\varepsilon_{1,k-1})$ is factorized into a product of $\varepsilon_{1,x}^{\frac{1}{2}}$ and $\phi^{(1)}(P/k)$, one gets

$$\phi^{(k)}(\underline{P}) \propto \{\int_0^\infty\cdots\int_0^\infty d\varepsilon_{1,1}\cdots d\varepsilon_{1,k-1}\ \prod_{x=1}^{k-1}\varepsilon_{1,x}^{\frac{1}{2}}\ h(E_d-\sum_{x=1}^{k}\varepsilon_{1,x})\}.[\phi^{(1)}(\underline{P}/k)]^k$$

$$\propto [\phi^{(1)}(\underline{P}/k)]^k \qquad (3.4.7)$$

From the asymptotic distribution functions of the atoms (see section 2)

$$dS/dE \propto E^{-n}f(\theta);\quad \phi(\underline{P}) \propto P^{-(2n+1)}f(\theta) \qquad (3.4.8)$$

the behaviour of the k-particle cluster distribution function at high energy is according to (3.4.7) and (2.2)

$$\phi^{(k)}(\underline{P}) \propto P^{-(2n+1)k}\ f^k(\theta)$$

$$dS/dE \propto E^{-kn-0.5(k-1)}\ f^k(\theta) \qquad (3.4.9)$$

For a heteronulear particle $X_{k_1}Y_{k_2}$ one finds in the same way for the high energy asymptote

$$\phi^{(k)}(\underline{P}) \propto P^{-(2n_1+1)k_1-(2n_2+1)k_2}\ f_1^{k_1}(\theta)\ f_2^{k_2}(\theta)$$

$$dS/dE \propto E^{-k_1n_1-k_1n_2-0.5(k_1+k_2-1)}\ f_1^{k_1}(\theta)\ f_2^{k_2}(\theta) \qquad (3.4.10)$$

where the index of n and $f(\theta)$ refers to the monomer distribution functions of X and Y.

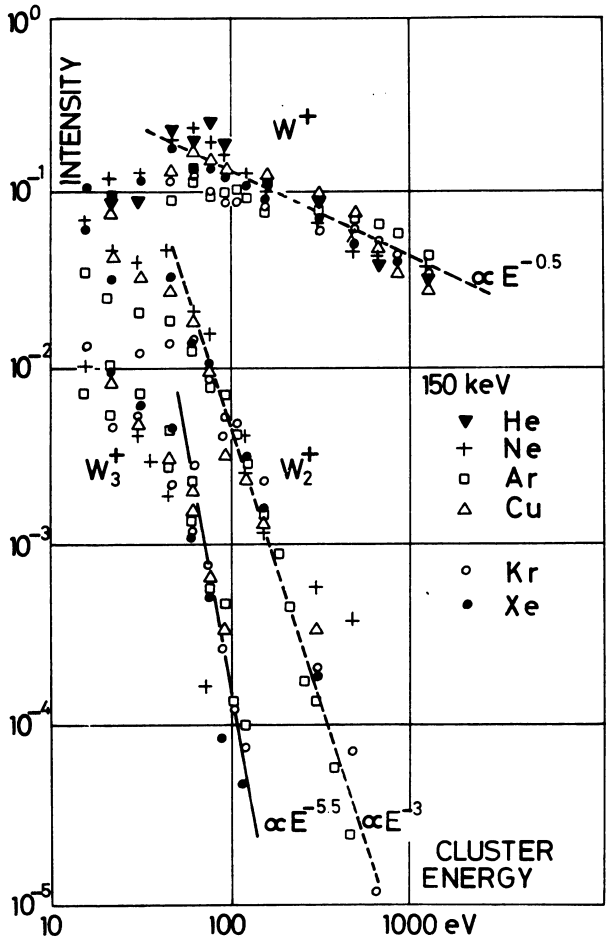

Fig. 3 - Energy distribution of W^+, W_2^+ and W_3^+ clusters, sputtered from a polycrystalline tungsten surface, as reported by Staudenmaier [2]. The dashed lines are the experimental E^{-n} energy distributions, the solid line represents the theoretical asymptotic behaviour for W_3^+.

4. COMPARISON WITH EXPERIMENTS

4.1 Asymptotic behaviour

Staudenmaier [2] reported the energy distributions dS/dE of some W_k^+ clusters, sputtered from a polycrystalline tungsten surface by bombardment with 150 keV He^+, Ne^+, Ar^+, Kr^+, Xe^+ and Cu^+ ions. The clusters were detected under 40^o with the surface normal. The energy spectra of W^+, W_2^+ and W_3^+ ions were measured over a wide energy range and showed an E^{-n} behaviour at higher energies.

Since the energy distribution of neutral W, sputtered from polycrystalline tungsten is not known, it is not possible to calculate the energy spectra of the cluster ions for the whole energy range. The asymptotic behaviour of the energy spectra at the high energy limit of W_k^+ ($k > 2$) and W_k however can be calculated from the reported W^+ and W_2^+ asymptotes according to formula (3.4.10). This of course implies that W_k^+ clusters are assumed to be formed from the association of one W^+ ion and k-1 W atoms, which are independently sputtered. From the reported values of n for W^+ and W_2^+ (0.5 and 3 respectively) one finds the W asymptote to be E^{-2}, which is the value to be expected from the sputtering theory [10,12]. The W_3^+ asymptote is found to be $E^{-5.5}$. Comparing this asymptotic behaviour with the experimental data of Staudenmaier, one concludes that the agreement is within the experimental error, as can be seen from figure 3.

Further measurements of Staudenmaier [13] enable us to test the predicted angular distributions of sputtered clusters in the high energy limit. Angular distributions of W_k^+ clusters ($k \leq 4$) were reported around the <111> direction of a tungsten single crystal (the surface normal being <110>) at 30 eV, and of W_k^+ ($k \leq 3$) at 60 eV. All W_k^+ clusters show a maximum intensity around the <111> direction. The predicted angular distributions of W_3^+ and W_4^+ clusters at 30 eV, calculated from the W^+ and W_2^+ distributions with (3.4.10), agreed well with the experimental data. The shape of the predicted W_3^+ curve at 60 eV agreed also with the experimental data, although its absolute value is somewhat lower than of the experimental points.

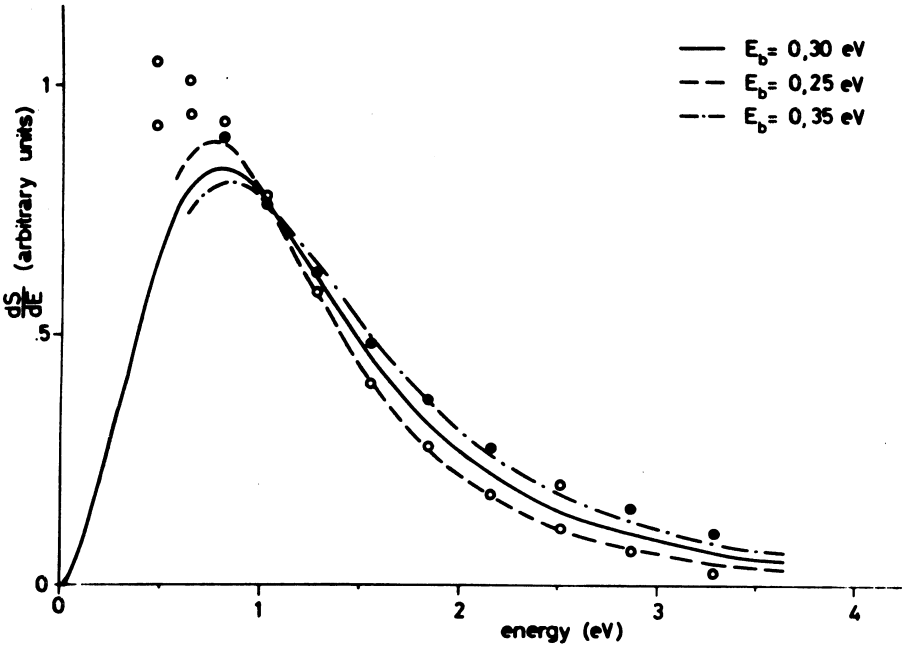

Fig. 4 - The energy distribution of K_2 dimers sputtered from a polycrystalline K target. The lines represent the theoretical curves with E_d = 0.55 eV, n = 1.525 and E_b = 0.25 eV, 0.30 eV and 0.35 eV. The open and closed circles are the experimental points of Baede et al., respectively with and without the two corrections discussed in the text. All curves have been normalized at 1.1 eV.

4.2 *Low energy spectra of dimers*

To compare the dimer formula with experimental data, one has to know the parameters E_b and n of the energy distribution of the monomers. However, only for the dimers K_2 and KI enough experimental data on the monomer distributions are available to make this comparison possible. In this section we will discuss these two cases.

4.2.1 *The K_2 distribution*

Baede, Jungmann and Los [6] measured the energy distribution of K_2 dimers sputtered from a polycrystalline K target under Ar^+ ion bombardment of 8, 11 and 13 keV kinetic energy. The sputtered K and K_2 neutrals were separated by an inhomogeneous magnet and measured by a surface ionization detector. The energy distribution of the dimers was found to be independent of the Ar^+ energy. The measured signals were corrected for scattering on the background gas. There were indications that part of the signal was due to reflected atoms. Assuming the number of dimers to be zero at 4 eV kinetic energy, the measured points were also corrected for this effect. However, since evidence was obtained from chemi-ionization experiments that alkali dimers are still present even at 5 eV kinetic energy, this last correction was considered to be too crude. The true K_2 spectrum was supposed to lie between the corrected and uncorrected points.

In the experimental set up of Baede et al. the particles were detected under an angle of 22.5° with respect to the normal of the target. However, the large Ar^+ current causes damage of the target surface after a short time so that the direction of the normal of the target becomes quite indefined. For the theoretical energy distribution we therefore used formula (2.6) and (2.2) for the normal direction.

In figure 4 the experimental points of Baede et al. are given. Since Baede reported the quantity $E \cdot \frac{dS}{dE}$ as a function of energy, his measured points have been divided by a factor E to obtain the energy distribution $\frac{dS}{dE}$.

The open and closed circles are the measured points of Baede

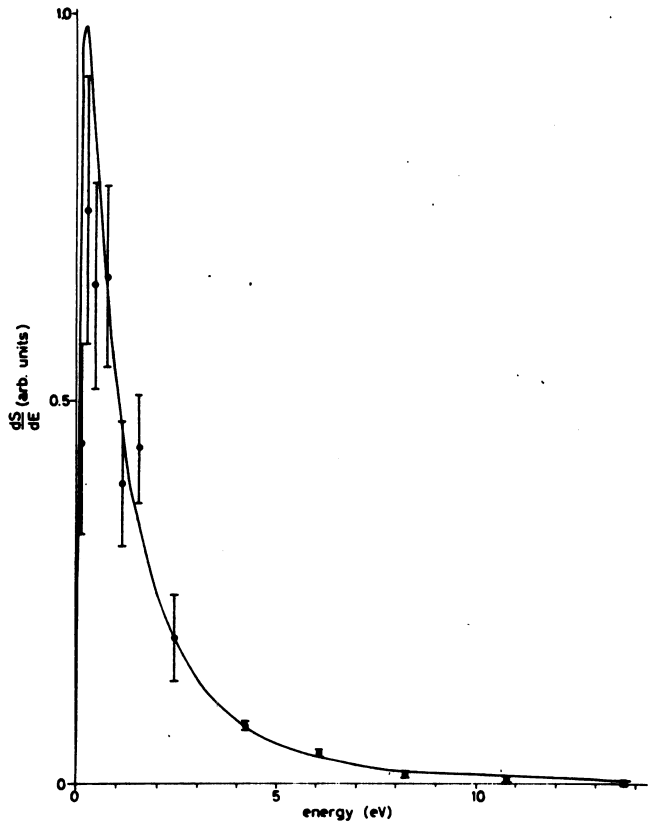

Fig. 5 - The energy distribution of KI. The solid line represents the sum of the theoretical curves with E_d = 3.0 eV, 1.1 eV and 0.6 eV. The parameters of the monomer distributions are n = 1.5, E_b = 0.2 eV for K and n = 2, E_b = 0.1 for I. The closed points are the experimental data. The curve has been normalized at 4.2 eV.

et al., with and without the corrections discussed above. The parameters of the monomer distribution are reported by Politiek and Kistemaker [9] (E_b = 0.71 and n = 1.525), the dissociation energy of K_2 in the gasphase is known to be 0.55 eV [14]. With these quantities the energy distribution could not be fitted with the theory. Taking however E_b = 0.3 eV, the theoretical curve coincides with the experimental points over a wide energy range. To demonstrate the sensitivity of the theoretical curve for changes in E_b, in figure 4 also the curves for E_b = 0.25 eV and E_b = 0.35 eV have been drawn. All curves have been normalized at 1.1 eV, as is the case in Baedes plot.

4.2.2 The KI energy distribution

Measurements of the energy distributions of K, I and KI sputtered in the normal direction of a polycrystalline KI target under 6 keV Ar^+ bombardment have been reported previously [7]. The parameter n was found to be 2 for I atoms and 1.5 for K atoms. The binding energy E_b of the atoms can be obtained by fitting the experimental curves with formula (2.3). This yields E_b = 0.7 eV and 0.4 eV for K and I atoms respectively.

The dissociation energy of KI molecules in the gasphase is 3.3 eV [14,15]. The closest distance R_o of K^+ and I^- ions in the lattice (3.5 Å [14]) is somwhat larger than the distance of K and I in the molecule (3.0 Å [15]). For this internuclear separation, the value E_d can be calculated to be 3.0 eV [15]. This difference however does hardly influence the shape of the theoretical energy distribution.

Contrary to the covalent molecule K_2, the potential energy of the ionic KI molecule has a very long range due to the coulombic attraction: this range extends to the crossing point of the covalent and the ionic potential curve in this molecule at 11.3 Å [16]. It can therefore be expected that sputtering of non-adjacent K and I atoms from the lattice gives also a contribution to dimer formation. The KI crystal has a fcc NaCl type structure. In this lattice, there are four possible configurations of K and I atoms with a distance below 11.3 Å, at 3.5, 6.6, 7.8 and 10.5 Å. From the coulombic potential the value of E_d for an internuclear separation of 6.6, 7.8 and 10.5 Å are calculated to be 1.1, 0.6 and 0.1 eV

respectively. The probabilities for sputtering a KI pair in either of the contributing configurations are taken to be equal. Evaluation of formula (2.6) then shows that K and I at 10.5 Å gives hardly any contribution to dimer formation, but the other configurations cannot be neglected.

In figure 5 the experimental energy distribution of KI is compared with the theory. The solid line represents the sum of the three contributions with E_d = 3.0 eV, E_d = 1.1 eV and E_d = 0.6 eV. The theoretical curve has been normalized by fitting it with the experimental point at 4.2 eV. Again, lower E_b values than expected have to be chosen to get the optimal fit to the theoretical curve with the experimental data. In figure 5, E_b = 0.2 and 0.1 eV for K and I respectively. Such changes in E_b however influence only the shape of the theoretical curve below 3 eV.

If only the contribution with E_d = 3.0 eV is taken into account, the resulting curve cannot be fitted with the experimental points above 3 eV for any choice of E_b. The sum of all contributions however agrees well with the experimental data, as can be seen from figure 5. From this it can be concluded that dimer formation from non-adjacent particles in the lattice is indeed important for ionic crystals.

5. CONCLUSION

The high energy results of section 4 indicate clearly that the present theory indeed explains the energy distributions of clusters. This means that clusters are formed by recombination of independently sputtered atoms, and that their energy distributions are determined by the E^{-n} power laws of the monomer distributions. Moreover, from the KI results it can be concluded that for ionic crystals various configurations of the atoms on the surface contribute to dimer formation. On the other hand, at the lowest energies there are deviations between theory and experiment, since the value of E_b in the dimer formula has to be chosen considerably lower than expected from the monomer distribution to get a fit with the experimental curves. This may indicate that the present theory under assumption V is a rather crude approximation. In fact, this

assumption states that the binding energy acts only upon the individual atoms of the cluster, thus decreasing both its initial center of mass energy and the relative motion in the cluster. It is likely however, that the binding energy plays a more complicated role in cluster formation. In many cases the atoms of the cluster originally have been quite close together on the surface, so that the sputtered aggregate closely resembles a molecule. Therefore it can be expected that part of the binding energy acts on the whole cluster, and does not influence the relative motion of the atoms in the cluster. Such refinements of the theory however will never change the asymptotic behaviour of the energy distribution at the high energy limit, since the binding energy can then always be neglected with respect to the kinetic energy of the cluster. This asymptotic behaviour remains therefore the same as in section (3.4), being only determined by the behaviour of the monomer distributions at high energy.

REFERENCES

[1] Z. Jurela and B. Perović, Can.J.Phys. 46 (1968) 773.

[2] G. Staudenmaier, Rad. Eff. 13 (1972) 87.

[3] E. Dennis and R.J. MacDonald, Rad.Eff. 13 (1972) 243.

[4] R.K.F. Herzog, W.P. Poschenrieder and F.G. Satkiewicz, Rad.Eff. 18 (1973) 199.

[5] F. Schmidt-Bleek, G. Ostrom and S. Datz, Rev.Sci.Instr. 40 (1969) 1351.

[6] A.P.M. Baede, W.F. Jungmann and J. Los, Physica 54 (1971) 459.

[7] G.P. Können, J. Grosser, A. Haring, A.E. de Vries and J. Kistemaker, to be published in Rad. Eff. (this thesis, chapter I).

[8] P. Joyes, J. Phys.B 4 (1971) L15.

[9] J. Politiek and J. Kistemaker, Rad.Eff. 2 (1969) 129.

[10] M.W. Thompson, Phil.Mag. 18 (1968) 377.

[11] G.P. Können, A. Tip, to be published.

[12] P. Sigmund, Phys.Rev. 184 (1969) 383.

[13] G. Staudenmaier, Rad.Eff. 18 (1973) 181.

[14] Handbook of Chemistry and Physics, 1972-1973.

[15] International tables of selected constants, part 17: Spectroscopic data relative to diatomic molecules, Ed. B. Rosen, Pergamon Press, New York 1970.

[16] A.C.M. Moutinho, J.A. Aten and J. Los, Physica 54 (1971) 471.

CHAPTER III*

NEGATIVE SURFACE IONIZATION OF HYPERTHERMAL HALOGEN ATOMS

Negative surface ionization of hyperthermal halogen atoms was studied as a function of their kinetic energy on thoriated tungsten and on niobium wires. The transition from a thermal equilibrium process to direct reflection causes the ionization to increase drastically above thermal energies: efficiencies up to 40% were found for 30 eV Cl atoms impinging on thoriated tungsten.

1. INTRODUCTION

Positive surface ionization (PSI) of atoms on surfaces is a well known phenomenon. It is used extensively for the measurement of particle fluxes in molecular beam experiments. Atoms striking the surface with thermal energies will stick to it for a time of about 10^{-4} - 10^{-3} sec. This is long enough to establish a thermodynamic equilibrium between the particles and the surface. The evaporation of ions is described by the well known Saha-Langmuir equation. For alkali atoms and hot surfaces with a high work function this results in an ionization efficiency of almost 100% [1]. At higher energies however a fraction of the impinging atoms is reflected directly, partly as ions, partly as neutrals. The latter particles cause a slight decrease in ionization efficiency with increasing energy [2,3]; reflected ions are formed even at the lowest temperature of the surface [4,5]. At energies of some tens of eV this "fast" ionization is the dominant mechanism of PSI, the efficiency is then almost independent of the temperature of the surface [6,7].

Negative surface ionization (NSI) is much less known. The ionization of molecules, containing atoms with high electron affinities, striking

* G.P. Können, J. Grosser, A. Haring and A.E. de Vries, Chem.Phys.Letters 21 (1973) 445.

a surface with a low work function at thermal energies, has been studied recently [8,9]. Even in the most favourable case the ionization efficiency is only 2%. For negative surface ionization, "fast" ionization at higher energies might increase the ionization efficiency. In this paper we report measurements on NSI of hyperthermal halogen atoms impinging on thoriated tungsten and niobium wires. We have found indeed that "fast" ionization occurs in this energy range with an efficiency which is an order of magnitude higher than NSI efficiency for thermal halogen compounds.

2. EXPERIMENTAL METHOD

A detailed description of the apparatus is given elsewhere [10]. Halogen beams were obtained by sputtering on alkalihalide (MX) surfaces with a 6 keV Ar^+ ion beam. After velocity selection the alkali component of the sputtered beam was measured by PSI on a Re 75μ Ø wire at 1400 K, giving currents of 5×10^{-14} to 2×10^{-13} A. At this temperature the ionization efficiency for thermal alkali beams is known to be unity even for Na because of oxidation of the wire [11]. The NSI detector on which the measurements for velocity selected halogens were performed, consisted of a wire surrounded by a cylindrical collector of 2 cm Ø. The wire was placed in a permanent magnetic field of 350 G to prevent electrons from reaching the collector. A potential difference of 30 to 60 V was maintained between wire and collector, so that energetic postive ions which may be formed on the wire could not reach the collector. The experiments were done with 100μ Ø Nb and 75μ Ø thoriated tungsten (W-Th) wires, the latter carbonized and activated according to Perski et al. [8]. We did not succeed in detecting low energetic sputtered halogens because the fluxes are low and because of the relatively high electron background at a temperature of 1600 to 1800 K at which most efficient NSI of thermal halogen compounds takes place [8]. For energies above some eV however, we found a temperature independent NSI signal. During the measurements of these hyperthermal halogens the temperature of the wire was kept at a temperature of 1300 K to avoid poisoning. At this temperature the electron background is negligible.

For the present research, halogen and alkali atoms were sputtered from MX targets with the lowest possible difference in mass between

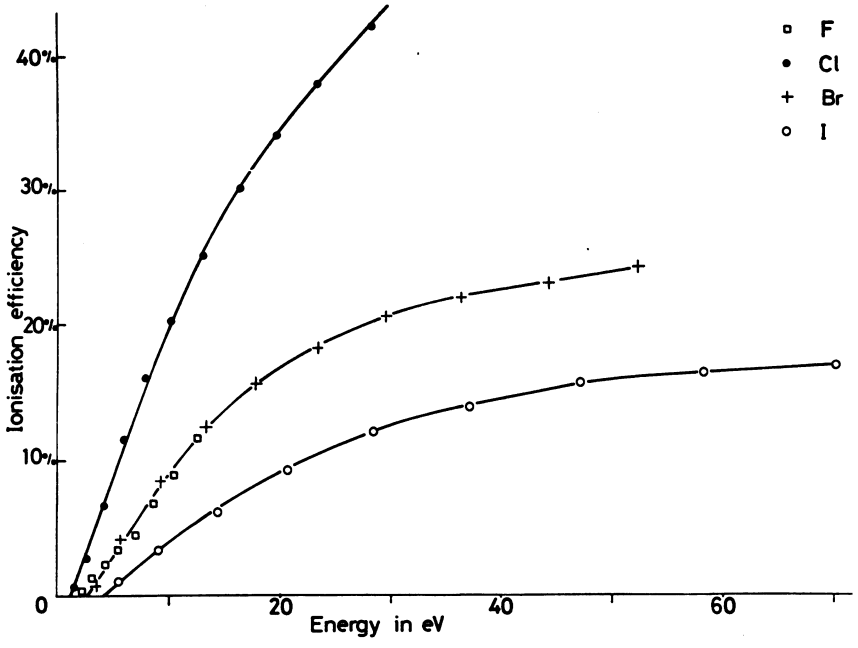

Fig. 1 - Negative surface ionization efficiency for F, Cl, Br and I atoms on thoriated tungsten as a function of their kinetic energy.

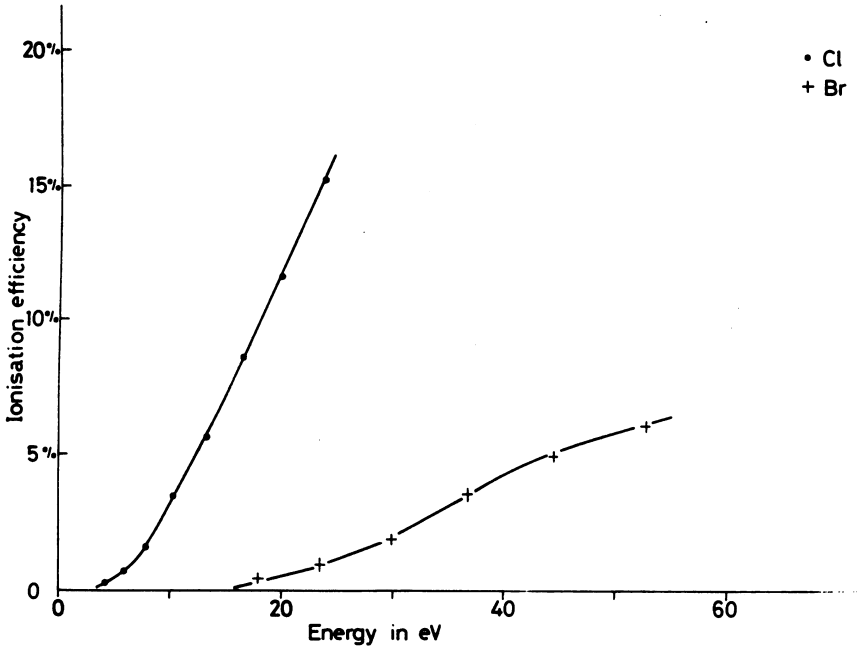

Fig. 2 - Negative surface ionization efficiency for Cl and Br atoms on niobium as a function of their kinetic energy.

the M and the X atom: NaF, KCl, RbBr and CsI. In earlier experiments the sputtered beam was analyzed by mass spectroscopy [10]. From these measurements we know that above a few eV the energy distributions of isobaric alkali and halogen atoms are the same.

From sputtering theory we infer that for the targets used by us at energies of some eV also the number of ejected alkali and halogen atoms is about equal [12].

Taking the PSI efficiency of energetic alkali atoms on Re to be unity, which may be true within 20% [2,3], the efficiency β of the NSI detector at a given energy is given by

$$\beta = (I^-/I^+)G, \tag{1}$$

in which I^- and I^+ are the signals on the NSI and PSI detector respectively, and G is a geometry factor. To determine G we reversed the potentials of the NSI detector and deactivated the W-Th wire. The PSI signal of a thermal K beam was now measured on both detectors. Because the ionization efficiency is known to be unity for K on deactivated W-Th and on Re [8,11], the ratio of these signals equals G. For Nb this measurement was done with thermal Cs. Because the work function of Nb and Re is higher than the ionization potential of Cs we assumed the ionization efficiency to be unity. The obtained values for G were in agreement with the calculated ones from the distances of the wires with respect to the source.

3. RESULTS AND DISCUSSION

In figures 1 and 2 the NSI efficiencies of the halogens on W-Th and on Nb wires are given as a function of energy. The NSI of F and I on Nb could not be measured, being lower than 1%. Because we used velocity selected beams, the maximum energy is different for the different halogens. Figures 1 and 2 show a dramatic increase of the efficiency, similar to that of the PSI of alkalis on cold surfaces [6,7].

Two remarks can be made concerning the results of figures 1 and 2. Firstly, it was found earlier that sputtered halogens are formed in the excited $^2P_{\frac{1}{2}}$ state for about 30 to 50% [10]. One might expect, that the NSI efficiency at a given energy will increase with

TABLE I

Electron affinities and measured ionization efficiencies on W-Th at 10 eV kinetic energy for different halogen atoms

	Electron affinity in eV [13]		Ionization efficiency at 10 eV kinetic energy
	$^2P_{1/2}$	$^2P_{3/2}$	
F	3.49	3.45	9%
Cl	3.72	3.61	20%
Br	3.82	3.36	9%
I	4.00	3.06	4%

increasing electron affinity of the atom and with decreasing work function of the detection wire. In table I the electron affinities of the halogens in the $^2P_{3/2}$ ground state and in the $^2P_{1/2}$ state are given as well as the ionization efficiencies at 10 eV kinetic energy on W-Th.

From table I we see that the ionization efficiencies show for F, Cl, Br and I the same tendency as the electron affinities of the $^2P_{3/2}$ ground state. From this we infer that the excitation does not play an important role in hyperthermal NSI.

Secondly, we found from our investigations on particles sputtered from various salt surfaces that MX molecules are present up to about 10 eV [10]. The maximum flux of these particles occurs at a few eV. At these velocities the flux of the MX molecules is about 30% of the halogen atoms. However, sputtering on all possible alkali chlorides, we found the same NSI signals as a function of velocity and the same thresholds [10]. Because the heavy MX molecules have relatively large energies at the threshold velocity, this indicates that highly efficient NSI of energetic molecules does not occur. This can be understood by the following arguments. The formation of MX^- is unlikely since the MX molecules have a closed shell configuration. An alternative mechanism for hyperthermal NSI would be dissociation of the MX molecules and formation of X^-, as is known to occur in NSI of thermal MX molecules. However, in thermal NSI the molecules are dissociated during the equilibrium with the surface, while reflected hyperthermal MX molecules have to take the dissociation energy directly from their kinetic energy. Therefore, the energy required for formation of X^- from hyperthermal MX on surfaces is much larger than for formation of X^- from X, and consequently the efficiency for the former process is expected to be very low. Finally, we want to mention the fact that the sputtered MX molecules can be detected on the PSI detector. For this reason the ionization efficiencies in figures 1 and 2 may be somewhat too low for energies below 5 eV.

REFERENCES

[1] M. Kaminski, Atomic and ionic impact phenomena on metal surfaces (Springer, Berlin, 1965).

[2] J. Politiek and J. Los, Rev.Sci.Instr. 40 (1969) 1576.

[3] J.F. Cuderman, Rev.Sci.Instr. 42 (1971) 583.

[4] R.P. Stein and F.C. Hurlbut, Phys.Rev. 123 (1961) 790.

[5] E. Hulpke and Ch. Schlier, Z.Physik 207 (1967) 294.

[6] A. Moutinho, Thesis, University of Leyden, The Netherlands (1971).

[7] R.K.B. Helbing and E.W. Rothe, J.Chem.Phys. 51 (1969) 1607.

[8] A. Perski, E.F. Greene and A. Kuppermann, J.Chem.Phys. 49 (1968) 2347

[9] M.J. Cardillo, M.S. Chou, E.F. Greene and D.B. Sheen, J.Chem.Phys. 54 (1971) 3054.

[10] G.P. Können, J. Grosser, A. Haring, A.E. de Vries and J. Kistemaker, to be published (this thesis chapter I).

[11] A. Perski, J.Chem.Phys. 50 (1969) 3835.

[12] P. Sigmund, Phys.Rev. 184 (1969) 383.

[13] Handbook for Chemistry and Physics (1972-1973);
C.E. Moore, Atomic energy levels, NBS Circular 467, Vol. 1 (1949), Vol. 2 (1952), Vol. 3 (1958) (US. Govt. Printing Office, Washington).

CHAPTER IV*

IONIZATION AND FRAGMENTATION OF ANILINE AND OTHER ORGANIC MOLECULES IN COLLISIONS WITH HALOGEN ATOMS IN THE ELECTRONVOLT ENERGY RANGE

Ionization and fragmentation of aniline, n-propylbenzene, carbon-tetrachloride, benzene, propane and cyclohexane is studied under halogen impact. The energy dependences of the ionization cross sections of aniline in collisions with halogens are reported. The results show an analogy with electron impact and photo-ionization mass spectroscopy. They are discussed in terms of potential curve crossings in the halogen organic molecule system.

1. INTRODUCTION

Since the electronvolt region has been opened for neutral atom beams, a number of papers has been published on the different aspects of collisional ionization. The research has been mainly restricted to alkali collisions with monatomic or diatomic particles [1]. In order to study fundamental chemical processes of organic molecules, we extended the sputtering technique to alkalihalide targets and thereby obtained hyperthermal halogen beams [2]. In the present paper we report measurements on the ionization and fragmentation of aniline ($C_6H_5NH_2$) and some other organic molecules in collision with these hyperthermal beams.

* G.P. Können, J. Grosser, A. Haring, F. Eerkens, A.E. de Vries and J. Kistemaker, Chem.Phys., to be published.

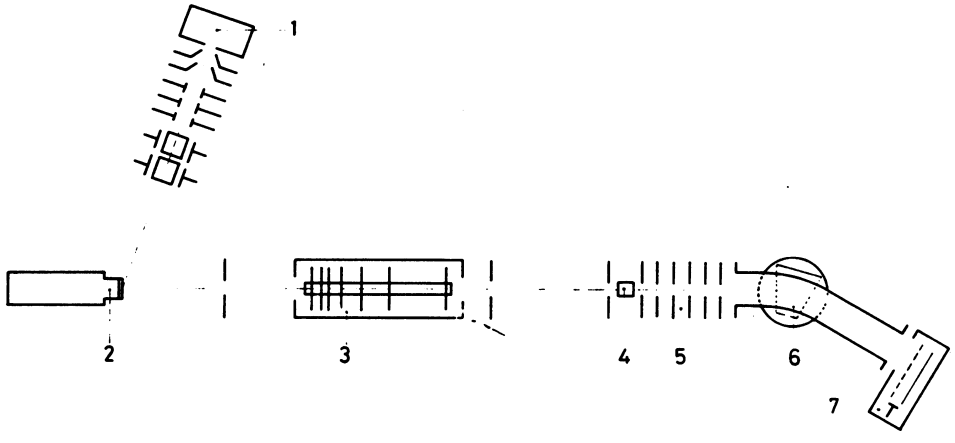

Fig. 1 - Schematic view of the apparatus. 1 ion source, 2 targetholder, 3 mechanical velocity selector, 4 collision region, 5 extraction field, 6 magnet, 7 multiplier.

2. EXPERIMENTAL METHOD

The apparatus used for the present experiments has been described previously in detail [2,3]. A schematic view of the relevant parts of this apparatus is given in figure 1. Neutral particles are sputtered from alkalihalide surfaces by a chopped 6 keV Ar^+ ion beam. After mechanical velocity selection and collimation they are crossed with a thermal beam. Ions formed in the collision center are extracted by a homogeneous electric field, pass a mass spectrometer and are counted on a particle multiplier with a forward-backward counter.

Data on the composition of beams sputtered from alkalihalide surfaces and on the energy dependence of the beam intensity have been reported earlier [2]. At the velocities which are required for the present experiments, the beam consists only of alkali and halogen atoms and a small amount of alkalihalide molecules. Evidence that the observed ions are only produced with the halogen constituent of the sputtered beam is taken from the fact that we find identical results with beams sputtered from NaCl, KCl or CsCl targets: Threshold velocities for collisional ionization with aniline ($C_6H_5NH_2$) are found to be the same within the experimental uncertainty for all these cases. Furthermore, the ion yields as a function of the velocity of the sputtered beam are identical for NaCl, KCl and CsCl. This is in agreement with our earlier statement [2] that the energy distributions of for instance Cl atoms sputtered from different alkalihalide surfaces are identical at eV energies. Another check consisted of producing a hyperthermal beam of potassium atoms by sputtering from a potassium target and crossing it with an aniline beam. Neither positive aniline ions nor positively charged fragments were observed in this case.

The thermal beam effuses from a multichannel array (channel diameter 12μ, channel length 480μ, surface 0.18 cm^2) and is shot directly into a liquid nitrogen trap. Typical working conditions in the mass spectrometer are: pressure before multichannel array 0.1 Torr, background pressure caused by the thermal beam 5.10^{-5} Torr, extraction voltage of the ions 1100 V. At working condition, the thermal beam has a small angular spread and the collision region is well defined.

The velocity selector has been calibrated by measuring the threshold of the process $K + Br_2 \rightarrow K^+ + Br^- + Br - 2.95$ eV [4].

TABLE I

(F, Cl, Br, I) aniline	93	66	52	39	28		
(NaCl) propane	42	28	15				
(NaCl) cyclohexane	85	56	41	28			
(KF, NaCl) carbontetrachloride	118	80	47				
(NaCl) benzene	79	64	52	39			
(NaCl) n-propyl benzene	121	91	78	66	51	39	28

Mass numbers of positive ions arising from collisions of halogen atoms with organic molecules. The targets which are used to generate the hyperthermal halogen beams are indicated in parentheses.

We estimated the error in the velocity calibration to be 0.3%. The resolution of the velocity selector $\Delta v/v$ is about 10%.

There are two instrumental effects which can cause errors in our results. Firstly, because of the poor resolution of the mass spectrometer ($m/\Delta m \sim 20$) the determination of the observed mass numbers is only correct within $\Delta m = \pm 1$. The exact values of the mass numbers of the measured ions were taken from the analogy with ordinary mass spectroscopy (see section 3.1). Although this procedure will be correct at low energies, where only a small number of fragment ions can be formed, it cannot be excluded that at higher energies a given mass spectrometer peak includes various neighbouring masses. No errors arise in connection with initial kinetic energy of the ions, and all ions of a given mass formed in the collision are indeed measured on the collector, as has been checked experimentally. Secondly, since there are also ionizing collisions in the acceleration field in the mass spectrometer, all peaks have a low intensity tail in the direction of lower mass numbers. It is probably due to this disturbing effect that some of the ions give a low positive signal below threshold. In most cases, it is negligible however. Small positive signals below threshold may also originate from collisions of sputtered alkalihalide molecules with the thermal beam.

3. RESULTS

3.1 Non-velocity selected spectra

Non-velocity selected beams of halogens X have been crossed with various thermal beams of organic molecules Y and the mass spectra of the formed positive ions have been recorded. The observed mass numbers are given in Table I. In parentheses the alkalihalide targets MX are indicated from which the halogens are sputtered. Fragment ions with mass near M could not be observed because they are obscured by the process $MX + Y \rightarrow M^+ + X^- + Y$. For aniline, only the halogen is indicated since for a given halogen several experiments have been done with various alkalihalide targets.

The mass numbers in Table I agree closely with the main singly charged fragments observed in electron mass spectroscopy [5]. No

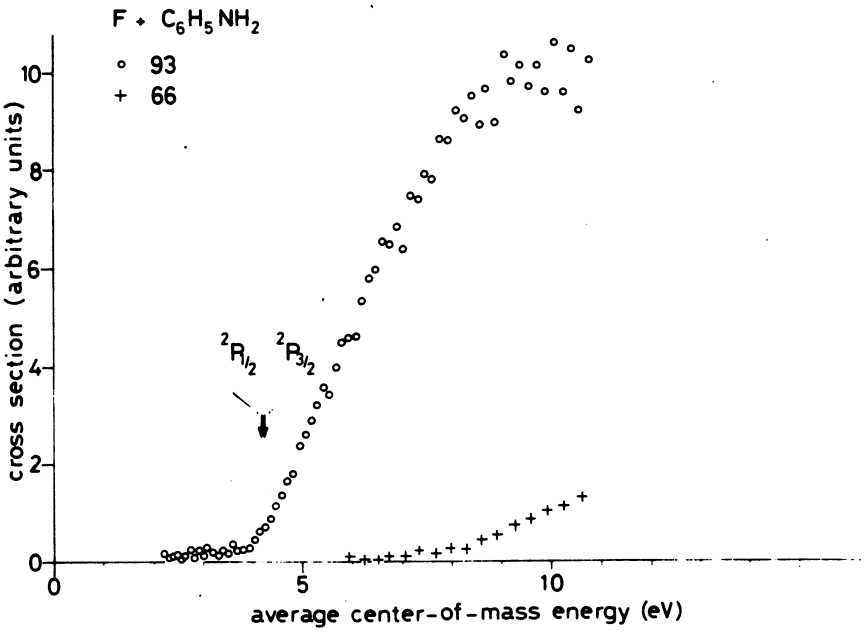

Fig. 2 - Cross sections for production of positive ions if F atoms collide on aniline. The centre of mass energy is averaged over the different isotope combinations. The mass 93 ion is the parent ion.

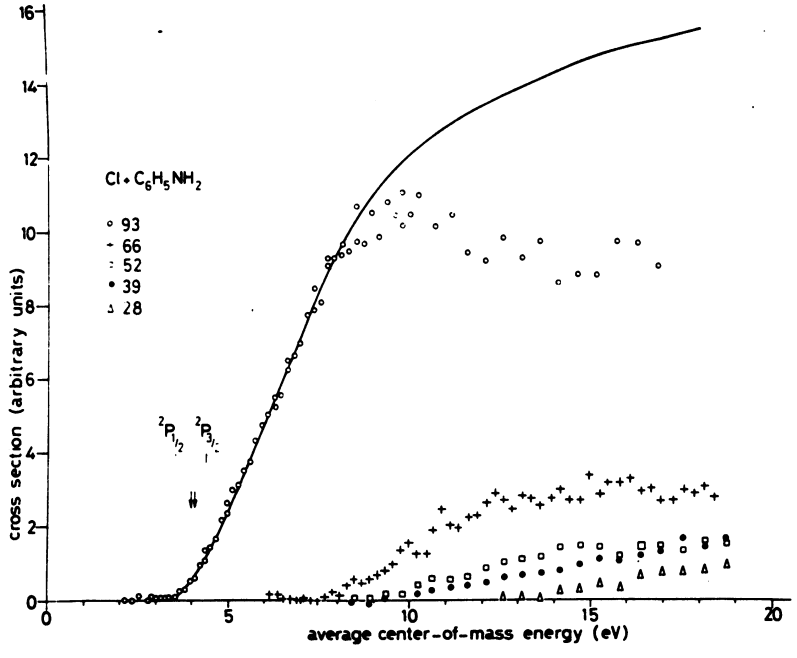

Fig. 3 - Cross sections for production of positive ions if Cl atoms collide on aniline. The centre of mass energy is averaged over the different isotope combinations. The gross ionization cross section (summed over all fragments) is indicated by a solid line. The mass 93 ion is the parent ion.

differences have been found in the mass numbers of the products arising from collisions with different halogens. This indicates that the processes occurring in halogen collisions are closely related to electron impact ionization and fragmentation. A similar relation seems to exist for negative ion formation, since alkali-SF_6 collision give rise to the same charged products as negative mass spectroscopy [6].

The relative intensities of the fragments are not given in Table I. Actually, these quantities cannot be compared entirely with the data of electron impact, since the measured ion yield of non-velocity selected beams is given by the convolution of the cross section with the energy distribution of the sputtered beam, which varies roughly with E^{-2} at electronvolt energies [2]. Nevertheless, the observed relative intensities show the same tendency as in electron impact.

3.2 Velocity selected spectra

The energy dependence of the ionization cross section of various positively charged fragments of the system F, Cl, Br and I with aniline ($C_6H_5NH_2$) are given in figures 2, 3, 4 and 5.

The solid line in figure 3 represents the gross ionization cross section, which is the sum over all fragments. For Br and I not all fragments could be measured because the signals were too low. The abscissa of the figures represent the center of mass energies of the halogen-aniline systems, calculated from the velocity of the sputtered beam and averaged over the naturally occurring isotopes. The energy dependence of the cross sections is obtained by dividing the counting rates by the flux of the sputtered beam. Flux distributions of Cl, Br and I have been measured directly [2]. For F sputtered from KF, the flux distribution was taken to be identical [2] to that of Na sputtered from NaCl. This latter distribution was measured by surface ionization detection. The experimental uncertainty in the flux distribution of the primary beams can cause an error of less than 20% in the cross sections at the higher energies in figures 2, 3, 4 and 5.

The height of the observed signals of the parent peak (mass 93)

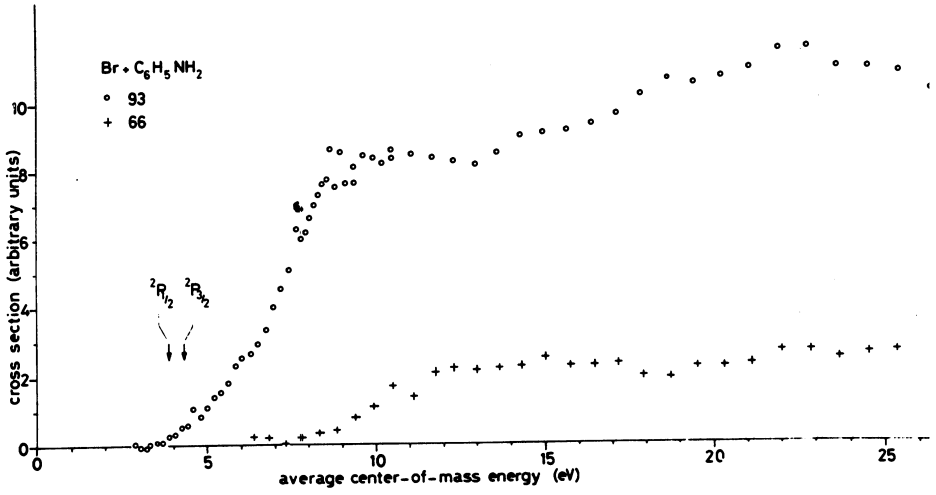

Fig. 4 - Cross section for production of positive aniline ions and the fragment ion with mass 66 if Br atoms collide on aniline. The centre of mass energy is averaged over the different isotope combinations.

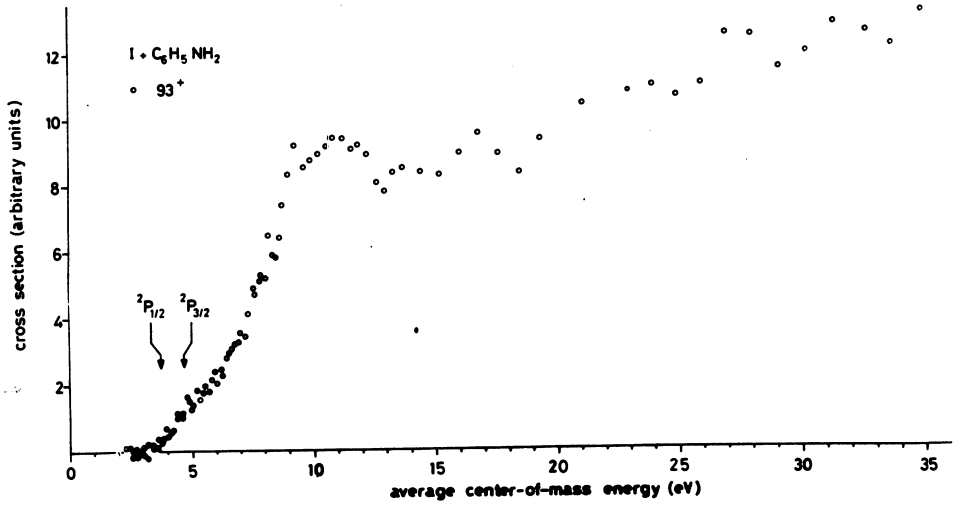

Fig. 5 - Cross section for production of positive aniline ions if I atoms collide on aniline. The centre of mass energy is averaged over the different isotope combinations.

decreases from F to I; the signals for F are about a factor of twenty higher than for I. From the flow of the sputtered beams we estimate the cross section to be in proportion to roughly 2 :1 : 0.5 : 0.3 for F : Cl : Br : I. Comparing the aniline signals with the signals obtained from the process $K + Br_2 \rightarrow K^+ + Br_2^-$ we estimate the ionization cross sections for Cl on aniline to be about 2% of the latter process at 7000 m/s. This corresponds with an absolute value in the order of 0.1 - 1 $Å^2$ [7].

The chemical composition of the fragments cannot be deduced from our experiments. From electron impact mass spectroscopy [8,9] one concludes that the products are mainly non-nitrogen containing compounds, originating from HCN loss. Although the mass 66 fragment in photoionization is reported to be an exception [10] a recent electron impact experiment [11] showed that also for low energies this fragment is a hydrocarbon. Adopting this result, the formula of the fragments with mass, 28, 39, 52 and 66 are $C_2H_4^+$, $C_3H_3^+$, $C_4H_4^+$ and $C_5H_6^+$, respectively.

Estimating roughly the thresholds for the parent peak in figures 2, 3, 4 and 5 we found them to be in good agreement with the values expected from the ionization potential of aniline [10] and the electron affinity of the halogens [12] in the cases of Cl and F. For Br and I however, the experimental thresholds were too low by about 0.4 and 1 eV respectively. We ascribe this effect to the presence of long lived $^2P_{\frac{1}{2}}$ excited halogens in the sputtered beam. The ground states are $^2P_{3/2}$. This explains both the agreement of the Cl and F results and the deviation of the Br and I threshold. The $^2P_{\frac{1}{2}}$ state lies 0.05, 0.11, 0.46 and 0.94 eV above the ground state of F, Cl, Br and I respectively [13]. From the fact that no signal is observed below the $^2P_{\frac{1}{2}}$ threshold we conclude that the $^2P_{\frac{1}{2}}$ atoms are the only excited halogen atoms in the beams.

3.3 Threshold energies

In this section first the various experimental effects that influence the threshold behaviour are discussed. Then we describe how the threshold energies are inferred from the experimental results; the values are reported in Table II.

It is assumed that the ideal ionization cross section for a certain halogen atom and aniline molecule as a function of the velocity is a straight line beginning at threshold. We define the threshold velocity of a process as the *principal threshold* if the following conditions are satisfied:

1) the thermal beam has zero velocity;
2) both colliding particles are in their ground state;
3) both particles have their most abundant mass number, so H = 1, C = 12, N = 14, F = 19, Cl = 35 and I = 127. We take however 80 in case of Br.

The *experimental threshold*, found by extrapolating the straight part of the cross section curve, will be shifted with respect to the principal threshold because of the following reasons:

1) Vibrational excitation of the molecules in the thermal beam. The thermal distribution of the vibrational states has to be known. For the aniline molecule, these were estimated from the known states of benzene [14].
2) Halogen projectiles in the metastable $^2P_{\frac{1}{2}}$ state. Since information is lacking, we assume that 50% of the halogen atoms are in the $^2P_{\frac{1}{2}}$ state. This will lead to an uncertainty of less than 0.1 eV in the thresholds. For I, the principal threshold was calculated from the $^2P_{\frac{1}{2}}$ threshold.
3) The velocity of the thermal beam. Its magnitude is known at room temperature, its angular spread can be neglected.
4) Isotope shift. The threshold velocity is different for different isotope combinations. The distribution of isotopes is well known for both colliding particles.

All these effects change the threshold velocity by at most a few percent, except in case of the Br and I metastables, as mentioned before. All combinations of masses and excited states (point 1, 2 and 4) have threshold velocities different from the principal threshold. For a delta-shaped velocity distribution the experimental ionization cross section $\sigma_1(v)$ will therefore be a superposition of several pieces of straight lines. If the slope of the cross section is supposed to be the same for all processes, the slope of $\sigma_1(v)$ is enlarged by an amount proportional to the probability of the new process at every new

threshold. This probability of course equals the relative abundance of the colliding particles from which the threshold is reached. Above the highest threshold, $\sigma_1(v)$ will be a straight line again. The extrapolation of this line will in general not intersect the x-axis at the principal threshold velocity.

To deduce the expected experimental cross section from $\sigma_1(v)$, this function has to be convoluted with the resolution function of the velocity selector, R(v). The resulting function will be called $\sigma_2(v_o)$, v_o being the nominal velocity of the selector. Thus

$$\sigma_2(v_o) = \int R(v)\ \sigma_1(v)\ dv \tag{1}$$

For mechanical velocity selectors, R(v) depends only on v/v_o [15]. Let R(v) be non-zero if $1-a < v/v_o < 1+b$, a and b being constants. Because of normalization one has

$$\int_{v_o(1-a)}^{v_o(1+b)} R(v)\ dv = 1 \tag{2}$$

On the right hand side of the threshold region, $\sigma_1(v)$ is a straight line. Let v_D be the intersection with the x-axis of its extrapolation. Then in this region we have $\sigma_1(v) \propto v-v_D$. Consequently one gets from (1):

$$\begin{aligned}
\sigma_2(v_o) &\propto \int_{v_o(1-a)}^{v_o(1+b)} (v-v_D)\ R(v)\ dv = \\
&= \int_{v_o(1-a)}^{v_o(1+b)} (v-v_o+v_o-v_D)\ R(v)\ dv \\
&= (v_o-v_D) \int_{v_o(1-a)}^{v_o(1+b)} R(v)\ dv + \int_{v_o(1-a)}^{v_o(1+b)} (v-v_o)\ R(v)\ dv \\
&= v_o-v_D + \int_{v_o(1-a)}^{v_o(1+b)} (v-v_o)\ R(v)\ dv
\end{aligned} \tag{3}$$

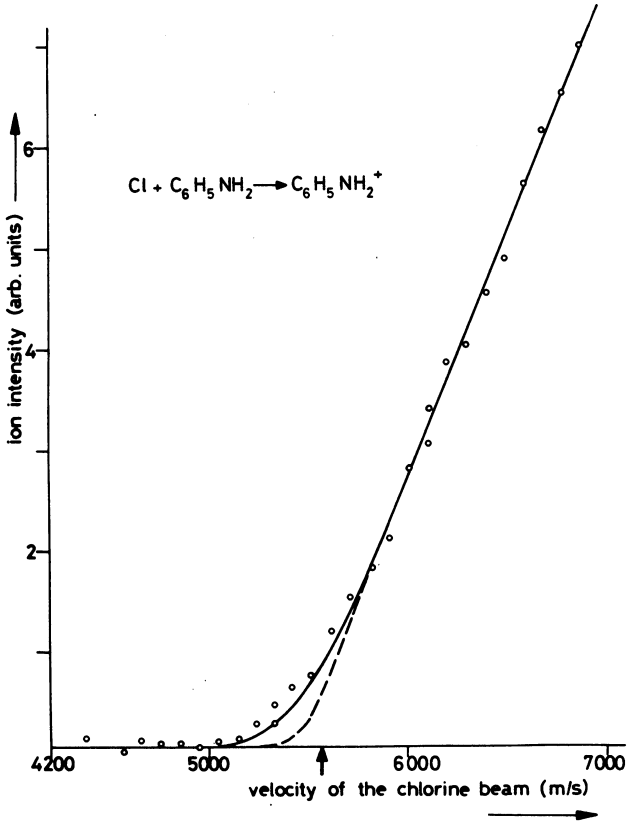

Fig. 6 - Comparison of the model cross section for Cl on aniline with the experimental results. The dashed line represents the effect of the presence of different isotope combinations and excited states of the colliding particles on the ideal linear cross section. The solid line is the convolution of this curve with the resolution function of the velocity selector. The principal threshold (see text) is indicated by an arrow. The circles are the experimental points.

Substituting in the remaining integral $w = v-v_o$, one finds

$$\sigma_2(v_o) \propto v_o - v_D + \int_{-av_o}^{bv_o} w\, R(v_o+w)\, dw \qquad (4)$$

The resolution function R(v) of the mechanical velocity selector is within a good approximation a symmetrical triangle around v_o [15]. This implies that a = b. Since in this case the integrand in (4) is anti-symmetric, the resulting integral is zero. So the intersection of the extrapolated straight part will be again v_D. The reported slight asymmetry in R(v) (a=0.10, b=0.11) will give rise to a negligible shift of the intersection of $\sigma_2(v_o)$ of about 0.3% of v_D to a higher velocity. This error however is entirely compensated by the fact that the calibration of the selector is also done with a known linear cross section. For the actual calculation of the threshold energy, the function $\sigma_1(v)$ was constructed, starting with a reasonably guessed principal threshold. The ratio of the principle threshold and the value at which the extrapolated straight part of $\sigma_1(v)$ intersects the x-axis was calculated; this latter intersection is identical to the intersection of $\sigma_2(v_o)$, as mentioned above. By multiplication of the experimental intersection with this ratio, the value of the principle threshold velocity and therefore of the energy is known.

In figure 6 the expected ionization yield $\sigma_2(v_o)$ is given for Cl and aniline as a solid line, together with a number of experimental points. $\sigma_2(v_o)$ is calculated by means of equation (1) with a triangular resolution function R(v) with $\Delta v/v$ = 10%. The dashed line in figure 6 is the function $\sigma_1(v)$, the expected cross section for a velocity selector with a δ shaped resolution function. The principal threshold, indicated by an arrow, lies to the right hand of the experimental threshold.

The slight difference between the predicted curve and the experimental points is due to the velocity and angular spread of the thermal beam and the non-ideal alignment of the velocity selector, causing a somewhat worse resolution. These effects however do not change the intersection. For some of the experimental curves, there remains a small positive signal below threshold. This was treated as background and subtracted. Of course, this enlarges the experimental uncertainty.

TABLE II

	F		Cl		Br		I		hν [10
Mass number	Threshold energy(eV)	Threshold + EA (eV)	Threshold energy(eV)	Threshold + EA (eV)	Threshold energy(eV)	Threshold + EA (eV)	Threshold energy(eV)	Threshold + EA (eV)	Threshold energy(eV
93	4.18±0.06	7.63±0.06	4.08±0.06	7.69±0.06	4.36±0.15	7.72±0.15	4.4 ±0.4	7.5 ±0.4	7.67±0.03
66	8.1 ±0.3	11.5±0.3	8.2 ±0.2	11.8±0.2	8.6 ±0.3	12.0±0.3	-	-	12.3±0.1
52	-	-	9.5 ±0.3	13.1±0.3	-	-	-	-	-
39	-	-	9.5 ±0.3	13.1±0.3	-	-	-	-	-
28	-	-	13.4±0.4	17.0±0.4	-	-	-	-	-

Threshold energies of charged fragments from ground state aniline ($C_6H_5NH_2$) formed by collisions with ground state halogen atoms and photons. In the second columns the electron affinity EA of the halogen atoms is added to the threshold energy.
EA is 3.45 eV for F, 3.61 eV for Cl, 3.36 eV for Br and 3.06 eV for I [12].

TABLE III

ion masses	17 eV Cl	70 eV e^- [5]
93	100	100
66	32	33
52	16	5
39	17	18
28	9	8

Relative intensities of charged fragments of aniline for 17 eV Cl impact and 70 eV electron impact.

In Table II the experimental values of the principal threshold energies are given, together with the values known from photo-ionization [10]. In the second column of the halogen results the electron affinity EA of the halogen atoms [12] has been added to the principal threshold. The values thus obtained represent the minimum energy which must be put into a ground state aniline molecule in order to ionize, giving either the parent ion or breaking it up into the observed fragment plus a neutral rest. In our case, this energy is partly provided by the relative kinetic energy and partly by the electron affinity of the halogen atom. The values of the sum of the threshold and the electron affinity can be compared directly with the appearance potentials from mass spectroscopy.

4. DISCUSSION

4.1 General

In Table III, the relative intensities of the various fragments of aniline formed in collisions with 17 eV Cl (our results) and 70 eV electrons [5] are compared.

These data are nearly equal, except for the mass 52 fragment. Due to the low resolution of the mass spectrometer in our experiment ($m/\Delta m \sim 20$), masses near the reported fragments might also give a contribution. At 17 eV it is likely that not all fragmentation thresholds will be reached. Therefore a simple mass spectrum of our aniline molecule can be expected. Consequently the mass peaks will have their main contribution from only one mass. The exception of mass 52 in Table III may however be due to a contribution of one or two fragments differing in mass only one or two mass units.

It is surprising that the fragmentation spectrum for both processes in Table III is so analogous. In case of electron impact it is believed that the only important variable for the fragmentation pattern is the amount of internal energy stored in the molecule. From Table III we get the impression that the 17 eV Cl projectile deposits about the same amount of energy into the target aniline molecule as a 70 eV electron. The former particle dissipates a large amount of its kinetic energy into excitation of the aniline,

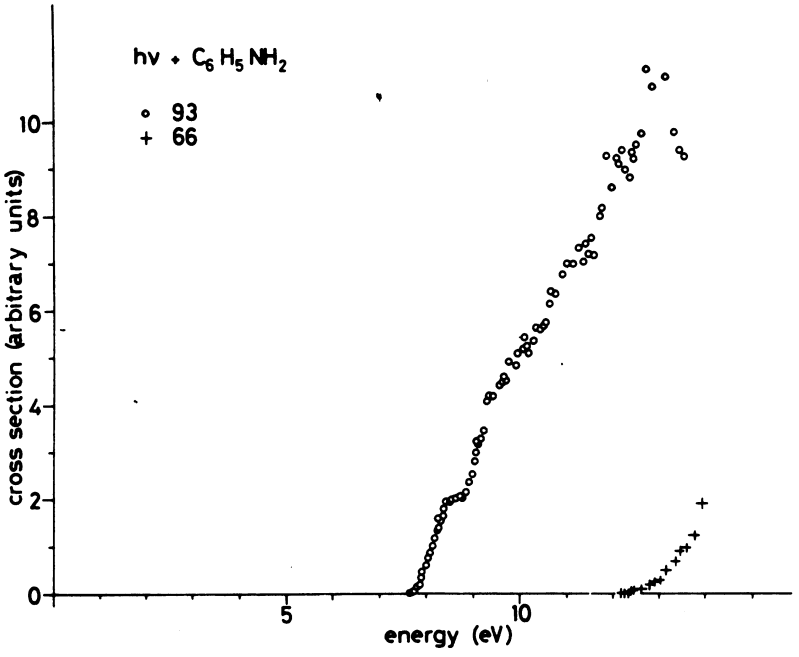

Fig. 7 - Photoionization cross section for aniline, as reported by Akopyan and Vilesov [10].

the electron of 70 eV only a small part.

Comparison with photon impact is instructive. Figure 7 shows the energy dependence of the photoionization cross section for the parent ion (mass 93) and the fragment ion with mass 66 for photon energies up to 14 eV, according to Akopyan and Vilesov [10]. The shape of the curves resembles our results (Figures 2, 3, 4 and 5). In Akopyans photoionization curve we notice some structure, contrary to our results. Our lack of structure cannot be entirely due to the finite energy resolution (1 eV) of our velocity selector. This difference will be treated in section 4.3. From the similar fragmentation results for the different processes (electrons, photons or halogen impact) we conclude that the formation of charged fragments in collisions with halogens proceeds in two steps. The first step is the formation of a positive molecular ion, which may contain excitation energy. Simultaneously a negative halogen ion is formed, as has been checked explicitly for Cl on aniline collisions up to 13 eV kinetic energy. The second step is a dissociative or radiative decay of the excited molecular ion, which also happens after the primary ionization by electron impact or photoionization. The possibility of dissociation of the molecular ion depends on its internal energy. In polyatomic ions vibrational and electronic energy quickly convert into each other via crossings of the potential hypersurfaces of the ion. The ultimate fragmentation takes place from a vibrationally excited ion [16,17]. This fragmentation is possible when the total available energy is larger than the dissociation energy of a particular bond. However, the energy might be distributed over different bonds and has to be concentrated in one bond to be broken. Therefore, contrary to diatomic molecules, the time needed for dissociation (10^{-8}sec.) is very long compared to the collision time (10^{-13} - 10^{-14} sec.). So the fragmentation pattern only depends on the total internal energy which is stored in the molecular ion [17]. This second step of the process has been discussed in many papers on the fragmentation of ions [16] and will not be treated further here. It occurs in exactly the same way with halogens as with electrons or photons. In the following we discuss the primary ionization and excitation processes of aniline molecules in collisions with halogens, because these processes are different from the photon and electron impact phenomena.

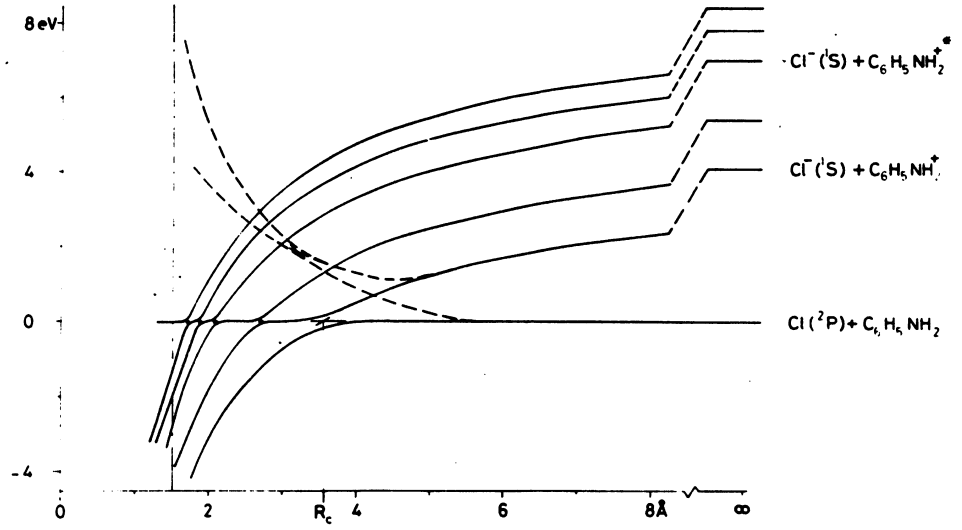

Fig. 8 - Schematic diagram of the potential energy curves in the Cl-aniline system. For the ionic curves, the ground state potential curve as well as the first four excited states of the aniline ion [22] are given. Internuclear repulsion is neglected; the vertical dashed line represents an estimate of the closest possible approach. Splittings due to spin have not been drawn. R_c is the crossing point of the two lowest potential curves. For these curves, the influence of repulsive forces is roughly sketched by the dashed curves.

4.2 Ionization and excitation process

In photon and electron impact ionization the primary process is electron excitation according to the Franck-Condon principle. This excitation can cause direct emission of an electron (ionization), possibly accompanied by simultaneous excitation of a second electron. In heavy particle collisions, the ionization and excitation of the colliding particles is assumed to take place at a crossing of the potential curves or hypersurfaces of the quasi-molecule. Such an explanation may be applicable also for complicated molecules.

In Figure 8 a schematic diagram is shown of the relevant adiabatic potential energy curves for the Cl-aniline system. The energy given refers to the vibrational ground state of the molecule. Only the Coulomb interaction has been taken into account, intermolecular repulsions and the connected splittings are neglected; splittings due to spin have also been omitted. The x-axis represents the distance between the centers of charge of the particles rather than the intermolecular distance. The vertical dashed line is an estimate of the closest possible approach for relative kinetic energies of about 10 eV. Of course, the real potential energy also depends on the orientation of the aniline molecule.

The ionic curves cross the neutral curve in a certain point; the crossing point of ground state ions with ground state molecules is indicated by R_c. If the colliding particles pass R_c one time adiabatically and one time diabatically, they separate as a Cl^- ion and a positive aniline ion in its electronic ground state. This can only happen if the kinetic energy is larger than the difference between the neutral curve and the asymptote of the ionic curve. In ion pair formation, this difference equals I-EA, I being the ionization potential of aniline molecules and EA the electron affinity of Cl atoms. For the formation of excited aniline ions, the system has to pass a second crossing point.

Repulsive forces will change the potential energy curves at short distances. This is schematically illustrated by the dashed curves in figure 8 for the two lower energy states. Due to this effect, the potential energy of the crossing points will become higher, and may even be larger than I-EA. In the latter case, the threshold for ionpair formation is also larger than I-EA, since the system has to pass the crossing point to form ions. Then,

just above threshold, the ionization cross section will be very small, since the classical turning point is near R_c. Consequently, the velocity at R_c is low and therefore the collision is almost completely adiabatic. Our curves however start at I-EA and have a steep rise immediately above threshold. Therefore in our systems the relevant crossing points lie below the asymptotes of the ionic curves.

In a complicated system like ours it is reasonable to assume that any of the crossing points can be passed both adiabatically and diabatically [17]. Of course, to get a transition, the kinetic energy has to be large enough to reach the crossing point. Therefore, crossings with very small internuclear separation will not contribute.

Little is known about the diabatic transition probability p at the crossing points. For simplicity, we consider the case that there are only two potential curves with one crossing point at R_c, where only radial coupling is relevant. Then, the transition probability is governed by the parameter $H_{12} = \langle 1|H|2\rangle$, in which $\langle 1|$ and $\langle 2|$ are the two diabatic electronic states and H is the electronic Hamiltonian. Generally, the diabatic transition probability increases with velocity. If H_{12} is small, the diabatic transition probability will have a large value even at low energy. If on the other hand H_{12} is large, diabatic transitions are only frequent at high energy. Depending on the symmetry of the system, H_{12} may be zero. If this is not the case, H_{12} depends mainly on the crossing distance R_c.

For the Cl-aniline system we have, neglecting the non-Coulombic forces: I = 7.7 eV, EA = 3.6 eV and $R_c = e^2/(I-EA) = 3.5$ Å. Calculating H_{12} as in the case of two atoms, we find $H_{12} = 0.5$ eV [18]. The Landau-Zener formula can give an idea about the transition probability for such a system at a given velocity v. From this formula it follows that if

$$\gamma \equiv 2\pi H_{12}^2/(\hbar v \frac{d}{dR}|H_{11}-H_{22}|_{R_c}) > 0.7$$

(H_{11} and H_{22} being the diabatic potential curves), the system behaves preferably adiabatically. At a crossing point of a Coulombic potential curve with a covalent one, $\frac{d}{dR}|H_{11}-H_{22}|_{R_c} = e^2/R_c^2$ if the non-Coulombic forces are neglected. Then, at a typical velocity of 10^4 m/s (13 eV Cl-aniline energy), γ is about 20. This means that

the diabatic transition probability will be small for such a system at eV energies.

In atom-molecule collisions, the symmetry of the system depends on the relative orientation of the colliding particles. It may therefore happen that H_{12} is small for a given orientation, but has a large value for other configurations. If the impact occurs near the orientation with a low H_{12} value, the diabatic transition probability will be large even at low energies. Therefore, the total ionization cross section at low energy might be larger than in the atomic case. This will result in a smaller energy dependence of the cross section for formation of ions in a specific internal energy state then in atom-atom ion pair formation. Thus, one may expect that the cross section for formation of aniline ions in a given vibrational state might be hardly energy dependent above its specific threshold. Then, the total cross section which represents the sum over all detailed cross sections is expected to be only considerably energy dependent near threshold, where new channels are opened with higher and higher internal energy of the aniline ion. Such a behaviour is indeed found experimentally in all aniline curves in figures 2-5.

In the one-dimensional approximation, the cross section σ for ion pair formation is given by $\sigma = 2\pi R_c^2 p(1-p)$ (p being the diabatic transition probability). The halogen-aniline cross sections are only a few percent of those for $K-Br_2$ at 7000 m/s, where $p \cong 0.5$ [7]. For $K-Br_2$, $R_c = 8$ Å [7]. From this, the diabatic transition probabilities in our systems can be calculated to be at most 5%. Therefore, the cross sections for formation of excited aniline ions are expected to be very small, since for this at least two crossing points have to be passed diabatically.

4.3 The influence of internal energy levels

Information about the amount of the total excitation energy of the ions can be obtained from the experimental results. In a very simplified model, one neglects the energy dependence of the cross section for formation of ions in a given internal state. Then, in ion pair formation each channel with a given internal energy has

an energy independent cross section above its specific threshold [19]. Within this model, the same holds for photoionization. The increase of the total ionization cross section is then only due to the population of new internal energy states of the ion. These states lie very closely together (<< 0.1 eV [14]) and thresholds will therefore not be resolved. Then the first derivative of the gross ionization cross section (summed over all fragments) is proportional to the distribution of the internal energy over the various excited states of the ions [20]. The gross ionization cross section is given for Cl on aniline by the solid line in figure 3. Since this cross section is nearly linear up to about 5 eV above threshold, it looks as if the distribution over the various internal energy levels is nearly uniform up to this energy. The further increase of the gross ionization cross section above 10 eV may be partly due to a trend of the detailed cross sections to increase. From the fact that new fragments are formed with thresholds up to 10 eV above the parent ion threshold it can however be concluded that aniline ions with internal energy up to 10 eV are produced. Since the increase of the gross ionization cross section above 10 eV is mainly caused by the fragments, one gets the impression that even in this energy range the detailed cross sections are not very dependent on energy. Therefore, the first derivative of the gross ionization cross section seems to approximate the internal energy distributions of the aniline ions even at higher energies.

It is unlikely that the internal excitation is formed by electronic excitation alone. As mentioned before, this would require more than one diabatic transition through a crossing point. Since in our system the crossing points are dominantly passed adiabatically, such a process has a low probability. On the other hand, the collision times (about 5.10^{-14}s for 13 eV Cl) are in the same order of magnitude as the vibration times in the molecule (about 3.10^{-14}s [14]), and vibrational excitation is thus a likely process. Part of the internal energy therefore is probably formed as vibration. Since multiquantum transitions take place at these energies even for di- and triatomic molecules [21], the total vibrational excitation of a complicated molecule like aniline may perhaps reach some eV's.

In photoionization, the vibrational levels are populated according to the Franck-Condon principle. The distribution function of the internal energy then shows a very marked structure [22]. Collisional excitation will be less selective and consequently the distribution function might be rather flat. Since the cross section equals roughly the integral of the internal energy distribution function, also no marked structure is to be expected in the ionization cross section. This corresponds with the absence of any structure in our measurements contrary to those at 8.4 eV in the photoionization curve.

As can be seen from Table II, the sum of the threshold energy for the mass 66 fragment and the electron affinity of the halogens is about 0.5 eV lower than the photoionization threshold. This latter value however equals the 66^+ threshold in electronbombardment [23]. This discrepancy might be understood as follows. Since the photoionization spectrum of aniline shows a maximum at 11.8 eV [22], it follows that in photoionization aniline ions with internal energy corresponding to the halogen process are indeed produced. If however the free conversion of the excited state corresponding to this maximum with lower levels is hindered, the mass 66 fragment will not be formed in photoionization, even though the energy content of the aniline ion is sufficient for formation of this fragment. In halogen collisions however, other states than in photoionization or electron bombardment ionization may be populated during collision, which do lead to production of the mass 66 fragment at our experimental thresholds.

REFERENCES

[1] A.P.M. Baede, to be published in Adv. in Chemical Physics.
J. Los in 'The Physics of Electronic and Atomic Collisions', VIII ICPEAC, Eds. B. Čobić and M.V. Kurepa, Beograd 1973 (Inst. of Physics. Beograd).
S. Wexler, Ber. Bunsengeseltschaft 77 (1973) 606.

[2] G.P. Können, J. Grosser, A. Haring, A.E. de Vries and J. Kistemaker, Rad.Eff., to be published. (this thesis, chapter I).

[3] J. Politiek, P.K. Rol, J. Los and P.G. Ikelaar, Rev.Sci.Instr. 39 (1968) 1147.

[4] A.P.M. Baede, D.J. Auerbach and J. Los, Physica 64 (1973) 134.

[5] American Petroleum Institute, Research number 44 "Catalog of mass spectra data".

[6] M.M. Hubers, private communication.

[7] A.P.M. Baede, J. Los, Physica 52 (1971) 422.

[8] P.N. Rylander, S. Meyerson, E.L. Eliël, J.D. McCollum, J.Am.Chem.Soc. 85 (1963) 2723.

[9] Mass Spectroscopy Data Centre AWRE, Aldermaston, Berks.

[10] M.E. Akopyan and V.I. Vilesov, Doklady Akademii Nauk SSSR, 158, (1964) 1386.

[11] N.M.M. Nibbering, private communication.

[12] Handbook of Chemistry and Physics, 1972-1973.

[13] C.E. Moore, Atomic Energy Levels, NBS Circulair 467, Vol. 1 (1949), Vol. 2 (1952), Vol. 3 (1958) (US Govnt. Printing Office, Washington).

[14] G. Herzberg, Infrared and Raman Spectra, van Nostrand comp., New York 1959.

[15] A.P.M. Moutinho, thesis, university of Leiden 1971.

[16] See, for example M.L. Vestal in "Fundamental Processes in Radiation Chemistry", Ed. P. Ausloos, Wiley Interscience Publishers 1970.

[17] B. Steiner, C.F. Giese, M. Ingram, J.Chem.Phys. 34 (1961) 189.

[18] R.E. Olson, F.T. Smith, E. Bauer, Appl.Optics 10 (1971) 1848.

[19] E.P. Wigner, Phys.Rev. 73 (1948) 1002.

[20] J.D. Morrison, J.Appl.Phys. 28 (1957) 1409.

[21] J.N. Bass, J.Chem.Phys. 60 (1974) 2913.
H. Udseth and C.F. Giese, J.Chem.Phys. 54 (1971) 3642.

[22] D.W. Turner "Molecular Photoelectron Spectroscopy", Wiley Interscience Publishers 1970.

[23] R. Frey and B. Brehm, private communication.

CHAPTER V*

ELECTRON TRANSFER AND REACTIVE IONIZATION IN C + O_2 COLLISIONS IN THE ELECTRONVOLT ENERGY RANGE

Cross sections for ion formation in C + O_2 collisions have been measured as a function of the kinetic energy up to 15 eV. Charge transfer is found to give rise to C^+, O_2^-, O^-, C^-, O_2^+ and free electrons. Five processes leading to these ions have been identified. Reactive ionization is taking place, proceeding according to three processes: $C + O_2 \rightarrow CO^+ + O + e^-$, $CO^+ + O^-$ and $CO + O^+ + e^-$.

1. INTRODUCTION

The development of atomic beam sources in the electron volt region about six years ago has led to an extensive study of charge transfer processes in atom-molecule collisions [1,2,3]. Especially the different aspects of alkali-halogen charge transfer processes have been the subject of investigation. Relatively unexplored however, are atom-molecule collisions in which no alkalis or halogens are involved. These systems are of interest since here ionization requires a close approach of the colliding particles, and reactive ionization is frequently observed [3,4,5].

Among the many possible collisional ionization experiments with non-alkalis which can be done, the system C + O_2 (see Table I) is of particular interest. Wexler [3], who studied angular distributions of positive ions formed in collisions of sputtered C atoms with O_2 molecules (however, without velocity selection of the C beam), found

* G.P. Können, A. Haring and A.E. de Vries, Chem.Phys.Letters, to be published.

TABLE I

	IP[11]	EA	$E_{diss}(25^{o}C)$[11]
C	11.26	1.27[17]	-
O	13.61	1.47[11]	-
O_2	12.06	0.43[16]	5.16
CO	14.01	-1.75[18]	11.14
C_2	12.0	3.54[12]	6.25

Ionization potentials (IP), electron affinities (EA) and dissociation energies E_{diss} of some C and O containing atoms and molecules. Values are expressed in eV.

that both C^+ and O_2^+ ions are formed. This indicates that in $C + O_2$ collisions two competing charge exchange processes are occurring, a feature that has never been observed before in any other system.

In this paper we report measurements on the various processes which take place in $C + O_2$ collisions as a function of energy up to 15 eV. It will be shown that besides the charge transfer processes various reactive ionization processes occur.

2. EXPERIMENTAL

2.1 The apparatus

The apparatus has been described previously [6]. A schematic diagram is given in figure 1. Particles are sputtered from a polycrystalline carbon target by a 6 keV Ar^+ ion beam, and after velocity selection and collimation crossed with a thermal oxygen beam. Charged particles formed in the $C + O_2$ collisions are accelerated in an electric field of 400 V/cm, pass a magnetic mass spectrometer and are counted on a particle multiplier. In order to reach the high velocities required for the present experiment, a larger velocity spread than usual was applied on the selector. The velocity selector was calibrated using aniline (An) as target gas, measuring $Cl + An \rightarrow Cl^- + An^+ - 4.08$ eV [7], which has a linear energy dependency of the ionization cross section. The resolution $\Delta v/v$ of the selector was determined to be 15%.

2.2 Carbon beams obtained by sputtering

The energy distribution $\frac{dS}{dE}$ of sputtered C atoms from polycrystalline targets is not yet known experimentally. In general however, after mechanical velocity selection, the flow of sputtered atoms is proportional to $E \cdot (dS/dE) \propto E^2/(E + E_b)^{n+1}$, in which E is the kinetic energy of the atoms, E_b the binding energy of the atom on the lattice (E_b = 7.4 eV for C [8]) and n is a constant between 1.5 and 2 [6,9,10]. Since this function varies only about 15% for C in the energy range in which the present experiments are done, the counting rates on the multiplier are considered to be proportional to the ionization cross sections.

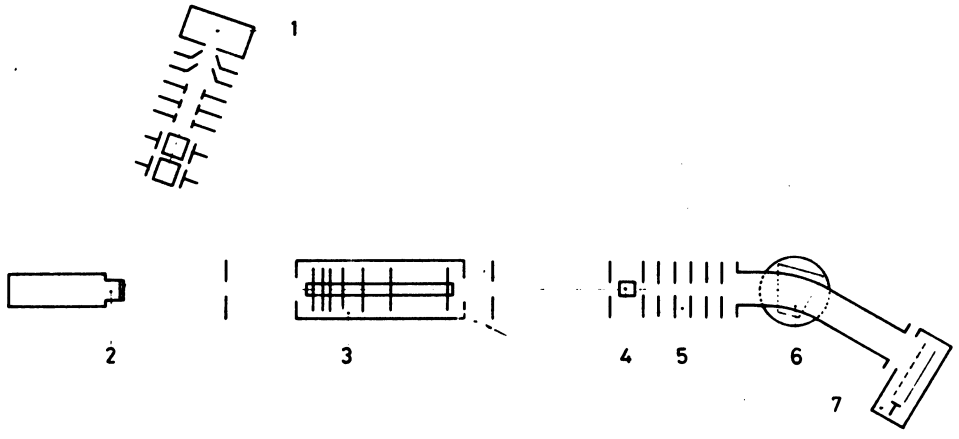

Fig. 1 - Schematic view of the apparatus. 1 ion source, 2 targetholder, 3 mechanical velocity selector, 4 collision region, 5 extraction field, 6 magnet, 7 multiplier.

It is to be expected that C_2 molecules (dissociation energy 6.24 eV [11]) and excited C atoms are also sputtered from the target. Indeed, crossing sputtered beams from C or WC targets with An, strong signals were observed from the process $C_2 + An \rightarrow C_2^- + An^+$. The intensities show a similar velocity dependence as the process $Cl + An \rightarrow Cl^- + An^+$. The threshold was determined to be 2.9 ± 0.1 eV. This means that C_2 molecules are present in the beam with an electron affinity EA of 4.8 ± 0.1 eV (the ionization potential of An is 7.7 eV). Since this value is considerably higher than the reported EA value of 3.54 eV [12], it may be that the sputtered C_2 molecules are partly in an excited state.

Crossing the sputtered beam with oxygen however, no trace of C_2^- or C_2^+ molecules was detected. Obviously, the ionization cross sections for $C_2 + O_2$ are negligible compared to $C + O_2$. Therefore in the interpretation of the data of the following sections the presence of C_2 is not considered.

C has two long lived excited states at low energies, the ^1D and the ^1S state, lying respectively 1.26 and 2.68 eV above the ^3P ground state [13]. One might expect that part of the sputtered C atoms are in this state. However, no shifts were observed in the thresholds of ions formed in $C + O_2$ collisions, which may be due to the presence of excited atoms. It is not clear if the ionization cross sections for these atoms are indeed so low, or that the excited atom is quenched before the ionizing collision takes place. A third explanation may be that the singlet states are simply not sputtered. A similar effect has been observed in neutralization of He^+ on Cu surfaces [14], in which only the triplet He states are populated. Finally it may be interesting to note that unselected beams sputtered from C targets showed positive surface ionization (PSI) on Re wires, being about 5% of the PSI signal obtained by K sputtering from K targets. This opens an opportunity to monitor sputtered C beams. Negative surface ionization on Nb surfaces, on the other hand was hardly observed; this signal was only 0.3% of the PSI signal of sputtered C.

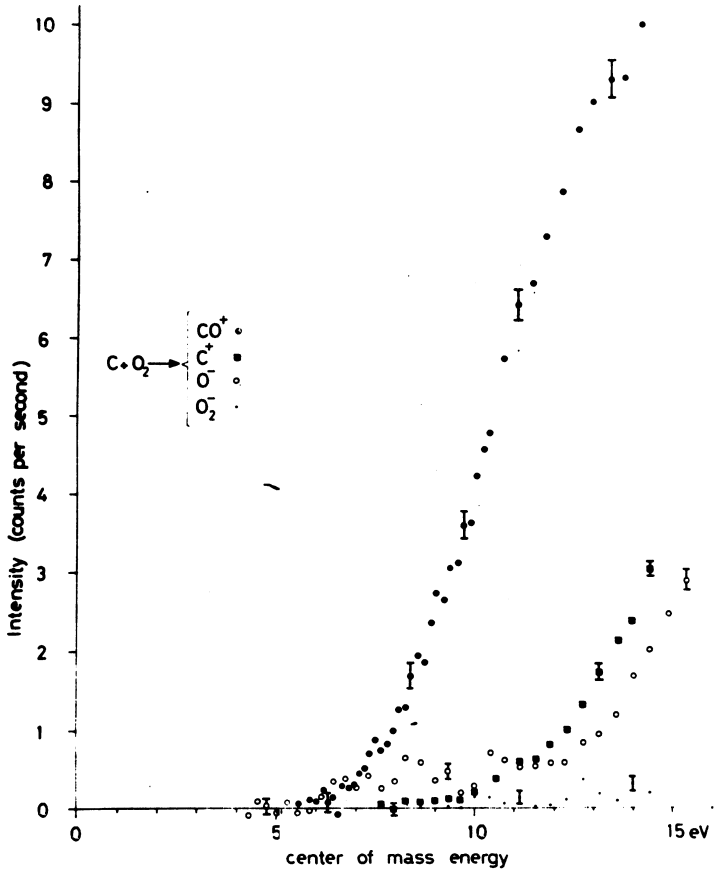

Fig. 2 - Production of C^+, CO^+, O^- and O_2^- ions in C + O_2 collisions as a function of the C - O_2 c.m. energy. The y axis represents the multiplier current in counts per second, which is in a good approximation proportional to the cross section (see section 2.2). For some experimental points, the statistical uncertainty has been indicated.

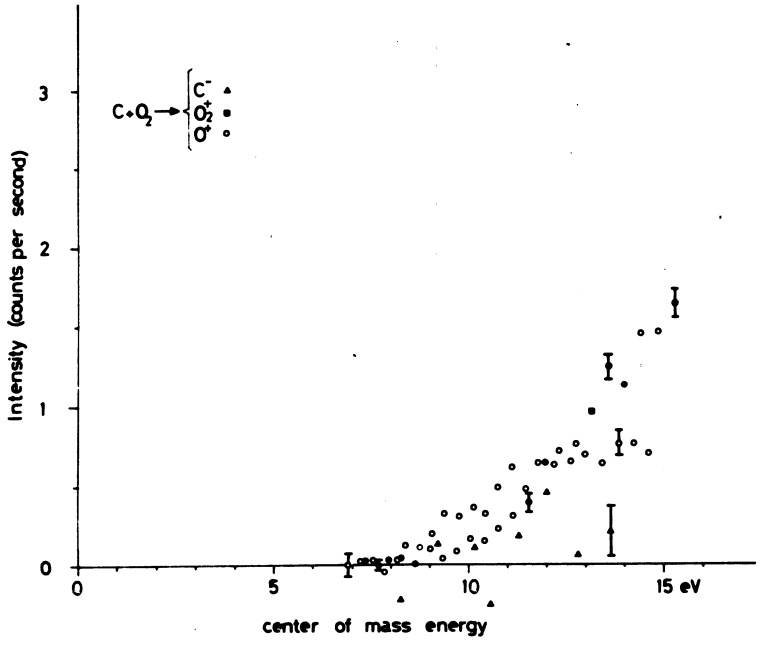

Fig. 3 - Production of C^-, O^+ and O_2^+ ions in C + O_2 collisions as a function of the C - O_2 c.m. energy. The y axis represents the multiplier current in counts per second, which is in a good approximation proportional to the cross section (see section 2.2). For some experimental points, the statistical uncertainty has been indicated.

3. RESULTS

In figures 2 and 3 the intensities of the ions formed in C + O_2 collisions are given as a function of energy. As has been mentioned before, the y axis is about proportional to the cross sections. Apart from the species C^+ and O_2^+, which are reported by Wexler [3], also C^-, O^+, O^-, O_2^+ and CO^+ ions are observed. From figures 2 and 3 it can be seen that the cross section for formation of positive ions is much higher than for formation of negative ions. This implies that also a considerable amount of free electrons is produced in C + O_2 collisions. In our system however, electrons cannot be detected directly.

Table II gives the relative intensities of all detected ions with a non-selected beam, and at 14.2 eV, together with the threshold energies. The relative intensities are accurate within 10%. Most thresholds were determined by fitting the experimental results with a linear model cross section (LF) which is convoluted with the resolution function of the velocity selector, as described previously [7]. The O^- curve however, gave no fit; here a step function model (SF) was used. The sharp increase at high energy in the O^- curve may reflect the onset of a new process. Its threshold was calculated by subtracting the signal at lower energies and fitting with the SF procedure. The thresholds for C^- and O_2^- production were not determined by fitting with a model cross section, since the signal to noise ratio of the experimental points is rather poor. Here, only a rough estimate is given (RE).

From the density of the O_2 beam and a rough estimate of the C beam flow we estimated that a signal of 10 c/s at the multiplier collector corresponds to a cross section in the order of 0.2 - 0.5 $Å^2$.

4. DISCUSSION

The charged products can be divided into two groups. Referring to the charge of the C ion, they will be called the *positive channel* and the *negative channel*. The positive channel leads to C^+, O^- O_2^- and CO^+ formation, the negative channel to C^-, O^+ and O_2^+. Figure 2 thus represents the positive channel and figure 3 the negative channel. From these figures and from Table II it follows that the

TABLE II

	Intensity unselected	Intensity 14.2 eV	E_{thr}(eV)
C^+	100	26	11.2 ± 0.2 (LF)
O^+	22	8	7.9 ± 0.3 (LF)
CO^+	45	100	7.9 ± 0.2 (LF)
O_2^+	38	13	10.6 ± 0.2 (LF)
C^-	13	3	11 ± 1 (RE)
O^-	52	18	6.5 ± 0.3 (SF)
			15.1 ± 0.3 (SF)
O_2^-	10	2.5	10.5 ± 1 (RE)

Relative intensities of the observed ions in C + O_2 collisions, with non-selected beams and at 14.2 eV c.m. energy. E_{thr} is the experimental threshold energy for the ions. LF and SF are thresholds found by fitting with a linear and a stepfunction model, RE are rough estimates (see text).

TABLE III

	Positive Channel		Negative Channel		
	C + O_2→	E_{thr}(eV)	C + O_2→	E_{thr}(eV)	
c1	$C^+ + O_2^-$	10.83	$C^- + O_2^+$	10.79	charge transfer
c2	$C^+ + O_2 + e^-$	11.26	$C + O_2^+ + e^-$	12.06	
c3	$C^+ + O^- + O$	14.95	$C^- + O^+ + O$	17.65	
r1	$CO^+ + O^-$	6.56	$CO^- + O^+$	9.38	reactive ionization
r2	$CO^+ + O + e^-$	8.03	$CO + O^+ + e^-$	7.68	

Calculated threshold energies for ionization processes in C + O_2 collisions.

negative channel has a considerably lower cross section than the positive channel. Table III gives the threshold energies for charge transfer and reactive ionization in both channels, calculated from the data of Table I. In this section we will discuss both channels separately and identify the processes occurring in $C + O_2$ collision with the aid of the tables and figures.

4.1 The positive channel

As can be seen in figure 2, the first peaks which appear in the positive channel are CO^+ and O^-. Up to about 7 eV signals have equal intensity. This implies that these ions originate from reaction r1 in Table III, $C + O_2 \rightarrow CO^+ + O^-$. Indeed, the threshold for O^- formation (Table II) agrees within the experimental error with the calculated threshold for $CO^+ + O^-$ formation as given in Table III. At higher energies, the CO^+ signal rises higher than the O^-. Apparently in this energy region, the reaction r2 ($C + O_2 \rightarrow CO^+ + O + e^-$) also takes place. At higher energies the cross section for r2 is much higher than for r1. The threshold for CO^+ formation, found by linear extrapolation (Table II) is mainly determined by process r2, and agrees within the experimental error with the theoretical value in Table III. If the O^- signal is subtracted from the CO^+ signal, the LF threshold of the resulting CO^+ curve then becomes about 8.0 eV, and is thus in agreement with its theoretical value for process r2.

Above 10 eV, also C^+ and O_2^- ions are formed. The O_2^- formation must be due to the charge transfer process c1, $C + O_2 \rightarrow C^+ + O_2^-$. The C^+ signal however rises much faster than the O_2^- indicating that C^+ ions are dominantly formed in process c2, $C + O_2 \rightarrow C^+ + O_2 + e^-$. The threshold for C^+ in Table II agrees with the theoretical value of this latter process. Finally, O^- shows a sharp increase at 13 eV. Of course, this effect may be due to an increase of the $CO^+ + O^-$ cross section. However, a fit of this increasing signal with the SF model yields a threshold of 15.1 eV (see Table II), which agrees within the experimental error with the theoretical value of process c3 giving $C^+ + O^- + O$. We therefore have the impression that this latter process is responsible for the increase of the O^- signal at high energies. Summarizing, it can be

concluded that all processes r1, r2, c1, c2, c3 contribute to ion formation in the positive channel.

As can be seen from figure 2, the O_2^- signal is very low compared to C^+. The whole C^+ curve however can be fitted with the LF model, yielding the threshold for the process $C + O_2 \rightarrow C^+ + O_2 + e^-$, and not for the energetically more favorable process $C + O_2 \rightarrow C^+ + O_2^-$, as can be seen from Tables II and III. This indicates that the "real" C^+ curve (measured with an ideal velocity selector with infinite resolution) behaves as follows; it has a low value between the $C^+ + O_2^-$ and $C^+ + O_2 + e^-$ thresholds and shows a sharp linear increase if this latter process becomes energetically possible. This behaviour is completely different from $K + O_2$ collisions, in which no such an increase in the total charge transfer cross section is observed at the $K^+ + O_2 + e^-$ threshold [15]. This is due to the fact that in this system the colliding particles separate as $K^+ + O_2^-$, after which free electrons may be formed by autoionization of vibrationally excited O_2^- ions. Therefore the charge transfer cross section reflects only the behaviour of $K^+ + O_2^-$ formation, since this autoionization is a secondary process. The sharp increase in the C^+ curve on the other hand indicates, that in this case the electrons are formed before the colliding particles separate as C^+ and O_2^-, thus if these particles are closely together. Contrary, at the energy where the channel $C^+ + O^- + O$ is opened, no extra increase in the C^+ curve is observed: the whole C^+ curve can be fitted with the LF model for $C^+ + O_2 + e^-$ formation. This means that the process $C + O_2 \rightarrow C^+ + O + O^-$ is related to $C^+ + O_2 + e^-$ formation, since O^- formation apparently occurs at the cost of electron formation.

The differences in behaviour in the charge transfer processes in $C + O_2$ and $K + O_2$ collisions can be understood as follows. In $C + O_2$ collisions, ionization requires a much closer approach of the colliding particles than in $K + O_2$, since the thresholds are much higher. Whereas the O_2^- formation can be described by Franck-Condon transitions in the O_2 potential curves in $K + O_2$ formation, this is not longer possible for $C + O_2$. It is known that C has a very strong chemical attraction to O_2. From the fact that reactive ionization has a large cross section in this system, it can be concluded that these attractive forces play a very dominant role in $C + O_2$ collisions. This means that these collisions have to be described on the whole system of

potential hypersurfaces of the CO_2 pseudomolecule as a three-body problem. The processes $C + O_2 \rightarrow C^+ + O_2^-$ and $C^+ + O_2 + e^-$ apparently describe very different paths on these hypersurfaces, which leads to the observed behaviour of the C^+ cross section curve.

The CO^+ threshold in Table II agrees with the process $C + O_2 \rightarrow CO^+ + O + e^-$. The weak O^- signal on the other hand reflects the process $C + O_2 \rightarrow CO^+ + O^-$. Apparently, the "real" CO^+ curve behaves like C^+: a low cross section between both thresholds and a steep rise above the second one. This indicates that free electron formation does not occur after the separation of CO^+ and O^- ions by autoionization of the O^- ion. Clearly also in this case the free electron is formed when the colliding particles are closely together. In this picture it is interesting that the $C + O_2 \rightarrow CO^+ + O^-$ cross section is hardly energy dependent, while the $C + O_2 \rightarrow CO^+ + O + e^-$ cross section shows a dramatic increase with energy in figure 2.

As can be seen from Table II and figure 2, the cross section for CO^+ formation at 14.2 eV is about a factor four higher than for C^+. In unselected beams however, the CO^+ signal is only fifty percent of the C^+ signal. This indicates that at very high energies the CO^+ cross section will become lower than the C^+ cross section. It is indeed to be expected that at high energies reactive ionization will have a small cross section, since the probability for rearrangement will be lower if the collision time is decreased. It may be that charge transfer processes like $C + O_2 \rightarrow C^+ + O_2 + e^-$ will take place when the process $C + O_2 \rightarrow CO^+ + O + e^-$ is not kinematically possible even at low energies.

No signal could be detected of the associative ionization process $C + O_2 \rightarrow CO_2^+ + e^- - 2.28$ eV. This is in contrast to the systems U, Ti, Ce, Ba + O_2 in which associative ionization has been observed [3,4,5].

4.2 The negative channel

In the negative channel, C^-, O^+ and O_2^+ ions are formed. Since the O_2^+ threshold lies below 11 eV, the process c1 ($C + O_2 \rightarrow C^- + O_2^+$) apparently contributes to the negative channel. From the experimental O_2^+ threshold we find an electron affinity of 1.5 eV for C atoms,

which is in agreement with the value given in Table I.

As can be seen from figure 3, the C^- signal is much lower than the O_2^+ signal for higher energies. This indicates that there is a considerable contribution of the process c2 ($C + O_2 \rightarrow C + O_2^+ + e^-$) in the negative channel. In contrast to the processes c1 and c2 in the positive channel, in this case the O_2^+ curve can be fitted with the LF model of the energetically most favourable process $C + O_2 \rightarrow C^- + O_2^+$. This indicates that the process c2 proceeds as follows: $C + O_2 \rightarrow C^- + O_2^+ \rightarrow C + O_2^+ + e^-$.

As can be seen from figure 3, O^+ ions are formed far below the threshold at 17.6 eV of process c3, giving $C^- + O^+ + O$. The experimental threshold for O^+ is even lower than for O_2^+. This can only be explained if O^+ ions are formed in one of the reactive ionization processes r1 or r2. From these two possibilities the $C + O_2 \rightarrow CO^- + O^+$ threshold is significantly higher than the experimental O^+ threshold. Therefore O^+ must be formed in the process r2: $C + O_2 \rightarrow CO + O^+ + e^-$. It can however not be excluded that at higher energies the process $C + O_2 \rightarrow CO^- + O^+$ also contributes to O^+ formation. CO^- ions are unstable and autoionize in a short time. Therefore they can never be detected on the multiplier.

Up to now, $C + O_2$ is the only system in which ionization in both the positive and negative channel is observed. Wexler [3] who only observed the C^+ and O_2^+ ions, assumed that these products are formed in both charge exchange processes c1 giving $C^+ + O_2^-$ and $C^- + O_2^+$ respectively. He suggested that the existence of both processes c1 is due to the low difference in the thresholds (10.83 eV and 10.79 eV respectively).

Our measurements however, indicate that C^+ is mainly formed in the process $C + O_2 \rightarrow C^+ + O_2 + e^-$. This does not mean however, that Wexlers argument is invalid. In fact, if the first step in the collision is a promotion of the system to the $C^+O_2^-$ or $C^-O_2^+$ hypersurface, after which electon loss or rearrangement takes place, Wexlers explanation can be applied. It is not impossible, however, that for the positive channel in which reactive ionization is so dominant, the first step is CO + O formation, after which ionization takes place. If this is the case, the existence of both channels might be correlated with the strong chemical interactions in the $C - O_2$ system. It would be interesting to see if a system like $Si - O_2$,

in which the three body interactions are expected to be analogous to C - O_2, also gives ionization in both channels.

REFERENCES

[1] A.P.M. Baede, to be published in Adv. in Chemical Physics.

[2] J. Los in 'The Physics of Electronic and Atomic Collisions', VIII ICPEAC, Eds. B. Čobić and M.V. Kurepa, Beograd 1973 (Inst. of Physics, Beograd).

[3] S. Wexler, Ber. Bunsengesellschaft, 77 (1973) 606.

[4] R.B. Cohen, E.K. Parks and S. Wexler, Chem.Phys.Letters 19 (1973) 99.

[5] W.L. Fite and P. Irving, J.Chem.Phys. 56 (1972) 4227.

[6] G.P. Können, J. Grosser, A. Haring. A.E. de Vries and J. Kistemaker, Rad.Eff., to be published (this thesis, chapter I).

[7] G.P. Können, J. Grosser, A. Haring, F. Eerkens, A.E. de Vries and J. Kistemaker, to be published (this thesis, chapter IV).

[8] Landolt Börnstein, Zahlenwerte und Funktionen, Band I, Teil 2, (Springer Verlag, 1960).

[9] M.W. Thompson, Phil.Mag. 18 (1968) 377.

[10] J. Politiek and J. Kistemaker, Rad.Eff. 2 (1969) 129.

[11] Handbook of Chemistry and Physics, 1972-1973.

[12] D. Feldmann, Z.f.Naturf. 25a (1970) 621.

[13] C.E. Moore, Atomic energy levels, NBS circular 467, Vol. I (1949), US Government Printing Office, Washington.

[14] C. Kerkdijk and E.W. Thomas, Physica 63 (1973) 577.

[15] A.C.M. Mountinho, J.A. Aten and J. Los, Physica 51 (1971) 432.

[16] R. Celotta, R. Bennet, J. Hall, J. Levine and M.W. Siegel, Abstract R3, 23nd Ann. Gaseous Electronics Conference, 1970.

[17] J.L. Hall and M.W. Siegel, J.Chem.Phys. 48 (1968) 944.

[18] J.M. Bardsley and F. Mandl, Rep.Progr.Phys. 31 (1968) 471.

SUMMARY

In this thesis an investigation is described which leads to the extension of hyperthermal atomic beam research to non-alkali systems. There are two lines in this thesis. The first one concerns the energy distributions of particles sputtered from solids and detection-possibilities of hyperthermal neutrals. The second one is a study of ionizing atom-molecule collisions in the electronvolt energy range.

Chapter I describes an experimental study of the energy distributions of particles sputtered from alkalihalide MX surfaces. Above a few eV the sputtered particles are almost exclusively atoms, so that in this energy range this technique can be applied to generate atomic halogen beams for collisional ionization experiments. At lower energies however also various molecules like MX and M_2X_2 are found to be sputtered. In addition, at thermal energies Maxwellian distributions are found due to the vaporization of the less effectively sputtered atoms from the surface. Excitation of sputtered halogens in the low lying $^2P_{\frac{1}{2}}$ states (0.05-0.9 eV above ground state) and of MX molecules has been observed. In Chapter II a model is developed to explain the energy distributions of sputtered clusters. It is assumed that clusters are formed by recombination of simultaneously sputtered atoms. The energy distribution function is given explicitely for sputtered dimers. For the energy distribution function of sputtered clusters at high energies a simple analytical expression is derived. Comparison with experimental results for W_k^+ ($k \leq 3$), K_2 and KI shows good agreement. For the ionic crystal KI, evidence is obtained that sputtering of non-adjacent K and I atoms from the lattice gives an important contribution to dimer formation. In Chapter III it is shown that negative surface ionization is an effective detection technique for hyperthermal halogen atoms. Ionization efficiencies up to 40% have been found, which is an order of magnitude higher than at thermal energies.

In Chapter IV the sputtered halogen beams are crossed with thermal beams of various organic molecules inside the ion source of a mass spectrometer to study the energy dependence of the ionization cross sections in these systems. It is found that

negative halogen atoms and positive organic molecular ions are formed. Fragmentation of organic molecular ions also takes place, the fragmentation patterns showing a strong analogy with electron impact and photoionization. Finally, in Chapter V the sputtering technique is extended to carbon, and ionization in $C + O_2$ collisions is studied. In this system, ionization takes place into two channels, leading essentially to C^+ and C^- formation. Five charge transfer processes have been identified. In addition, three reactive ionization processes are found. It is concluded that in this system the covalent forces between the particles play an important role in the ionization processes.

S A M E N V A T T I N G

Dit proefschrift beschrijft een onderzoek, dat geleid heeft tot uitbreiding van het botsingsonderzoek van atomen en moleculen in het electronvolt gebied voor niet-alkali's. Het onderzoek kan in twee delen worden gesplitst. Het eerste betreft de energieverdelingen van deeltjes die ontstaan bij kathodeverstuiving van vaste stoffen en de detectiemogelijkheden van niet-alkali's. Het tweede deel handelt over ionisatieprocessen die optreden bij botsingen tussen atomen en moleculen met energieën in het electronvolt gebied.

In Hoofdstuk I is een experimenteel onderzoek beschreven naar de energieverdelingen en samenstelling van bundels die van alkalihalogenide (MX) oppervlakken verstoven zijn. Het blijkt dat boven enkele electronvolts deze bundels practisch alleen uit atomen bestaan. Hieruit volgt dat de verstuivingstechniek in dit energie gebied goed toepasbaar is voor het maken van atomaire halogeenbundels ten behoeve van botsingsonderzoek. Beneden deze energieën bevat de bundel echter ook moleculen van de vorm MX en M_2X_2. Bovendien zijn in het thermische gebied Maxwellverdelingen gemeten, die veroorzaakt worden door verdamping van die atomen, die het minst effectief verstoven worden. Het is gebleken dat zowel de halogeenatomen als de MX moleculen zich in aangeslagen toestanden kunnen bevinden. Aangezien bij de halogenen slechts het laagste niveau bevolkt is, bedraagt de aanslag energie hier ten hoogste één electronvolt. In Hoofdstuk II wordt een theoretisch model uitgewerkt om de energieverdelingen van verstoven moleculen te verklaren. Hierbij wordt er van uitgegaan dat het bombarderen van oppervlakken primair emissie van atomen ten gevolge heeft. Indien de relatieve kinetische energie van een aantal gelijktijdig verstoven atomen echter lager is dan hun onderlinge bindingsenergie, zullen deze atomen recombineren en aldus tot molecuulvorming aanleiding geven. Voor tweeatomige moleculen wordt expliciet de energieverdeling gegeven, die op grond van dit model te verwachten is. Tevens wordt voor hoge energieën de energieverdeling van willekeurig grote moleculen afgeleid; dit blijkt een eenvoudige analytische uitdrukking te zijn. De berekende energieverdelingen blijken goed overeen te komen met de waargenomen verdelingen van W_k^+ ($k \leq 3$), K_2 en KI. Bovendien is gevonden dat voor het ionogene

kristal KI recombinatie van K en I atomen die geen naaste buur in het kristal vormen een niet te verwaarlozen bijdrage tot de dimeerformatie geeft. In Hoofdstuk III wordt aangetoond dat boventhermische halogeenatomen zeer efficient gedetecteerd kunnen worden door middel van negatieve oppervlakteionisatie. In het gunstigste geval is een ionisatieopbrengst van 40% gemeten, hetgeen een orde groter is dan bij thermische energieën.

In Hoofdstuk IV wordt een onderzoek beschreven over bundels van verstoven halogeenatomen die worden gekruist met thermische bundels van verschillende organische moleculen. Hierbij is de energieafhankelijkheid van de ionisatiedoorsneden bestudeerd. Het blijkt dat bij deze botsingen ladingsoverdracht tussen de botsende deeltjes optreedt, hetgeen leidt tot de vorming van negatieve halogeen ionen en positieve organische molecuulionen. Deze laatste dissocieren gedeeltelijk in kleinere brokstukken. Het fragmentatiepatroon van de molecuulionen vertoont een sterke overeenkomst met de fragmentatiepatronen die ontstaan in fotoionisatie en bij beschieting door electronen. Tenslotte wordt in Hoofdstuk V de kathode verstuivingstechniek uitgebreid tot koolstof. In dit hoofdstuk worden metingen gerapporteerd van de ionisatieprocessen die optreden bij beschieting van O_2 moleculen door atomaire koolstof. In dit systeem vindt ionisatie plaats naar twee kanalen; deze leiden in principe tot C^+ en tot C^- formatie. Er konden vijf verschillende processen worden geïdentificeerd, waarin een electronensprong optreedt tussen de koolstofatomen en de zuurstofmoleculen. Bovendien zijn er drie reactieve ionisatieprocessen waargenomen, waarbij dus tevens een zuustofatoom wordt uitgewisseld. Uit deze metingen kan worden geconcludeerd dat in dit soort systemen de covalente krachten tussen de botsende deeltjes een belangrijke rol spelen in de ionisatieprocessen.